INFLUENCE OF FINITE RADIAL GEOMETRY ON COHERENT RADIATION GENERATION BY A RELATIVISTIC ELECTRON BEAM IN A LONGITUDINAL MAGNETIC WIGGLER

Ronald C. Davidson

and

Yuan-Zhao Yin

PFC/JA-84-23 June, 1984

INFLUENCE OF FINITE RADIAL GEOMETRY ON COHERENT RADIATION GENERATION BY A RELATIVISTIC ELECTRON BEAM IN A LONGITUDINAL MAGNETIC WIGGLER

Ronald C. Davidson†
Plasma Research Institute
Science Applications Inc.
Boulder, CO, 80302

Yuan-Zhao Yin*
Plasma Fusion Center
Massachusetts Institute of Technology
Cambridge, MA, 02139

ABSTRACT

The influence of finite radial geometry on the longitudinal wiggler free electron laser instability is investigated for TE mode perturbations about a uniform density electron beam with radius $\hat{R}_b$. The equilibrium and stability analysis is carried out for a thin, tenuous electron beam propagating down the axis of a multiple-mirror (undulator) magnetic field $\underset{\sim}{B}_0(\underset{\sim}{x}) \simeq B_0[1+(\delta B/B_0)\sin k_0 z]\hat{\underset{\sim}{e}}_z$, where $\lambda_0=2\pi/k_0=$const. is the wiggler wavelength. It is assumed that $k_0^2\hat{R}_b^2<<1$, and that perturbations are about the self-consistent Vlasov equilibrium $f_b^0(\underset{\sim}{x},\underset{\sim}{p})=(\hat{n}_b/\pi)\delta(p_\perp^2-2\gamma_b m\omega_b P_\theta-2\gamma_b m\hat{T}_{\perp b})\times\delta(p_z-\gamma_b mV_b)$, where $p_\perp^2=p_r^2+p_\theta^2$, P_θ is the canonical angular momentum, and $\hat{n}_b$, γ_b, ω_b, $\hat{T}_{\perp b}$ and V_b are positive constants. For $\delta B/B_0<<1$ and slow beam rotation ($\omega_b<<\omega_{cb}=eB_0/\gamma_b mc$), the equilibrium density is uniform ($\hat{n}_b$) out to the beam radius $\hat{R}_b=(2\hat{T}_{\perp b}/\gamma_b m\omega_b\omega_{cb})^{1/2}$. Detailed free electron laser stability properties are investigated for the case where the amplifying radiation field has TE-mode polarization with perturbed field components ($\delta\hat{E}_\theta$, $\delta\hat{B}_r$, $\delta\hat{B}_z$). The matrix dispersion equation is analyzed in the diagonal approximation, and it is shown that the positioning of the beam radius ($\hat{R}_b$) relative to the conducting wall radius (R_c) can have a large influence on the growth rate and detailed stability properties. Analytic and numerical studies show that the growth rate increases as $\hat{R}_b/R_c$ is increased.

---

† Permanent Address: Plasma Fusion Center, Massachusetts Institute of Technology, Cambridge, MA 02139.

* Permanent Address: Institute of Electron, Academia Sinica, Beijing, People's Republic of China.

I. INTRODUCTION AND SUMMARY

There have been several theoretical[1-26] and experimental[27-35] investigations of coherent radiation generation by free electron lasers that use an intense relativistic electron beam as an energy source. Both longitudinal[1-5] and transverse[6-18] wiggler magnetic field geometries have been considered, and there have been many theoretical estimates of the gain (growth rate) that treat the system as infinite and uniform transverse to the beam propagation direction. Few calculations,[5,16,17] however, have attempted to include the important influence of finite radial geometry in a fully self-consistent manner, and these analyses[5,16,17] have indicated that the relative positioning of electron beam radius ($\hat{R}_b$) to conducting wall radius (R_c) can indeed have a large effect on the linear growth rate and the detailed stability properties.

The longitudinal magnetic wiggler configuration[1-4] has been identified[1] as a strong candidate for coherent radiation generation at frequencies significantly higher than those generated by the cyclotron maser instability (assuming the same average axial field B_0). In the present article, we investigate the influence of finite radial geometry on the longitudinal wiggler free electron laser instability.[1-4] The analysis is carried out for a thin, tenuous electron beam propagating down the axis of a multiple-mirror (undulator) magnetic field (Sec. II and Fig. 1). It is assumed that $k_0^2\hat{R}_b^2 \ll 1$ and that the amplifying radiation field has TE-mode polarization with perturbed field components ($\hat{\delta E}_\theta$, $\hat{\delta B}_r$, $\hat{\delta B}_z$). Here, $\hat{R}_b$ is the beam radius, $\lambda_0 = 2\pi/k_0 = \text{const.}$ is the wavelength of the wiggle in the axial magnetic field, and the conducting wall is located at radius $r = R_c$. A very important feature of the linear stability analysis (Secs. III and IV) is that the positioning of the beam radius relative to the conducting

wall radius (as measured by $\hat{R}_b/R_c$, say) can have a large influence on the growth rate and detailed stability properties relative to the case where the system is treated as infinite and uniform[1] in the transverse direction.

To briefly summarize, in Sec. II we describe the equilibrium properties of a thin, tenuous electron beam propagating down the axis of a multiple-mirror magnetic field. Equilibrium self fields are neglected, and the vacuum magnetic field is approximated by [Eq. (3)][1]

$$B_z^0(r,z) = B_0\left[1 + \frac{\delta B}{B_0}\sin k_0 z\right],$$

$$B_r^0(r,z) = 0,$$

for $k_0^2\hat{R}_b^2 \ll 1$. Beam equilibrium properties ($\partial/\partial t = 0$) are investigated for the choice of self-consistent equilibrium distribution function [Eq. (6)][36]

$$f_b^0(\underset{\sim}{x},\underset{\sim}{p}) = \frac{\hat{n}_b}{\pi}\,\delta(p_\perp^2 - 2\gamma_b m\omega_b P_\theta - 2\gamma_b m\hat{T}_{\perp b})\,\delta(p_z - \gamma_b m V_b),$$

where $p_\perp^2 = p_r^2 + p_\theta^2$, p_z is the axial momentum, P_θ is the canonical angular momentum, and $\hat{n}_b$, γ_b, ω_b, $\hat{T}_{\perp b}$ and V_b are positive constants. Here $\gamma_b mc^2$ is the characteristic energy of a beam electron. For <u>small</u> wiggler amplitude ($\delta B/B_0 \ll 1$) and a <u>slowly rotating</u> electron beam with $\omega_b \ll \omega_{cb} = eB_0/\gamma_b mc$, it is found that $f_b^0(\underset{\sim}{x},\underset{\sim}{p})$ can be approximated by [Eq. (16)]

$$f_b^0(\underset{\sim}{x},\underset{\sim}{p}) = \frac{\hat{n}_b}{\pi}\,\delta\left[p_\perp^2 - (\gamma_b m\hat{V}_{\perp b})^2(1 - r^2/\hat{R}_b^2)\right]\delta(p_z - \gamma_b m V_b),$$

where $\hat{V}_{\perp b}^2 = 2\hat{T}_{\perp b}/\gamma_b m$. In this case, the axial modulation of the beam envelope is negligibly small with $R_b(z) \simeq \hat{R}_b = \text{const.}$ [Eqs. (10) and (14)], and the beam density is <u>uniform</u> with $n_b^0(r) = \hat{n}_b$ over the interval $0 < r < \hat{R}_b$ [Eq. (9)]. The particle trajectories in the equilibrium field configuration (3) are also described in Sec. II [Eqs. (17)-(20)].

Stability properties are investigated in Secs. III and IV for TE-mode perturbations about the choice of self-consistent solid-beam equilibrium specified in Eq. (16). Assuming perturbed field components $(\hat{\delta E}_\theta, \hat{\delta B}_r, \hat{\delta B}_z)$, the linearized Vlasov-Maxwell equations [Eqs. (24)-(25)] are analyzed using techniques established in recent investigations[37-39] of the influence of finite radial geometry on the cyclotron maser instability. In particular, for a tenuous electron beam, we approximate the r-depencence of $\hat{\delta E}_\theta(r,z)$ by the vacuum waveguide solution, $J_1(\alpha_{0\ell} r/R_c)$, where $\alpha_{0\ell}$ is the ℓ'th zero of $J_1(\alpha_{0\ell}) = 0$ [Eq. (30)]. After considerable algebraic manipulation, this gives the matrix dispersion equation [Eq. (43)]

$$\left\{\left(\frac{\omega^2}{c^2} - k^2 - \frac{\alpha_{0\ell}^2}{R_c^2}\right) + \sum_{n=-\infty}^{\infty} \chi_{n,n}(k,\omega)\right\} \tilde{\delta E}_\theta(k)$$

$$+ \sum_{N\neq 0}^{\infty} \sum_{n=-\infty}^{\infty} \chi_{n-N,n}(k+Nk_0,\omega)\, \tilde{\delta E}_\theta(k+Nk_0) = 0,$$

where the susceptibility $\chi_{m,n}(k,\omega)$ is defined in Eq. (50) for the choice of radially confined equilibrium distribution $f_b^0(\underset{\sim}{x},\underset{\sim}{p})$ in Eq. (16). For sufficiently small wiggler amplitude, the off-diagonal terms in Eq. (43) can be neglected, and the dispersion relation is approximated by [Eq. (47)]

$$\left(\frac{\omega^2}{c^2} - k^2 - \frac{\alpha_{0\ell}^2}{R_c^2}\right) + \sum_{n=-\infty}^{\infty} \chi_{n,n}(k,\omega) = 0.$$

The striking feature of the definition of $\chi_{m,n}(k,\omega)$ in Eq. (50) is the strong dependence of the integrand on radial coordinate r. For the case of small energy variation over the beam cross section, we obtain the approximate expression for $\chi_{n,n}(k,\omega)$ given by [Eq. (55)].

$$\chi_{n,n}(k,\omega) = -\frac{1}{4}\frac{\omega_{pb}^2}{c^2} J_n^2\left(\frac{\omega_{cb}}{k_0 V_b}\frac{\delta B}{B_0}\right)$$

$$\times \left\{\left(\frac{g_1 f_1(\omega)}{[\omega-(k+nk_0)V_b-\omega_{cb}]} - \frac{\hat{V}_{\perp b}^2}{c^2}\frac{g_2 f_2(\omega)}{[\omega-(k+nk_0)V_b-\omega_{cb}]^2}\right)\right.$$

$$\left. + \left(\omega_{cb} \to -\omega_{cb}\right)\right\} ,$$

where $f_1(\omega)$ and $f_2(\omega)$ are defined in Eqs. (56) and (57), and g_1 and g_2 are the geometric factors defined in Eqs. (53) and (54) (see also Fig. 2).

In Sec. IV, we obtain approximate analytic and numerical solutions to the diagonal dispersion relation (47) for $\chi_{n,n}(k,\omega)$ specified by Eq. (55). Several points are noteworthy from the stability analysis. First, for a given harmonic number n, the characteristic maximum growth rate [Eq. (68)] is largest whenever the argument of J_n corresponds to the first zero of $J_n'(x) = 0$, i.e., when

$$\frac{\omega_{cb}}{k_0 V_b}\frac{\delta B}{B_0} = \alpha_{n,1} ,$$

where $\alpha_{n,1}$ is the first zero of $J_n'(x) = 0$. Second, the characteristic maximum growth rate scales as $(\hat{V}_{\perp b}/c)^{2/3}\hat{n}_b^{1/3}$, which can lead to substantial gain for the longitudinal wiggler free electron laser. Third, there is a strong dependence of stability properties on the positioning of the beam radius ($\hat{R}_b$) relative to the conducting wall radius (R_c). In particular, the growth rate $\mathrm{Im}\omega$ increases as $\hat{R}_b/R_c$ is increased, and the detailed dependence of $\mathrm{Im}\omega$ on $\hat{R}_b/R_c$ is examined numerically in Sec. IV. Another important feature of the results is

that the instability is inherently broadband in the sense that many harmonics are unstable, even when $(\omega_{cb}/k_0 V_b)(\delta B/B_0)$ is chosen to maximize emission for a particular value of n.

Finally, also in Sec. IV, we investigate stability properties in the limiting case where $\delta B = 0$. This corresponds to the cyclotron maser instability for perturbations about the solid electron beam equilibrium $f_b^0(\underset{\sim}{x},\underset{\sim}{p})$ specified by Eq. (16). The numerical results for $\delta B = 0$ also show a strong dependence on radial geometry $(\hat{R}_b/R_c)$.

II. EQUILIBRIUM MODEL AND ASSUMPTIONS

A. Equilibrium Field Configuration

In the present analysis, a tenuous electron beam propagates along the axis of a multiple-mirror (undulator) magnetic field with axial periodicity length $\lambda_0 = 2\pi/k_0$ and axial and radial vacuum magnetic fields, $B_z^0(r,z)$ and $B_r^0(r,z)$, given by[1]

$$B_z^0(r,z) = B_0\left[1 + \frac{\delta B}{B_0} I_0(k_0 r)\sin k_0 z\right] ,$$

$$B_r^0(r,z) = -\delta B I_1(k_0 r)\cos k_0 z , \tag{1}$$

where $I_n(k_0 r)$ is the modified Bessel function of the first kind of order n, and $\delta B/B_0 < 1$ is related to the mirror ratio R by $R = (1+\delta B/B_0)/(1-\delta B/B_0)$. In circumstances where the beam radius R_b is sufficiently small that

$$k_0^2 R_b^2 << 1, \tag{2}$$

and the oscillatory field amplitude δB is small with $\delta B/B_0 < 1$, then the leading-order oscillation (wiggle) in the applied field is primarily in the axial direction, with $B_r^0 = O(k_0 r \delta B/B_0) B_z^0$. Within the context of Eq. (2), the equilibrium magnetic field components can be approximated by[1]

$$B_z^0(r,z) = B_0\left[1 + \frac{\delta B}{B_0}\sin k_0 z\right] ,$$

$$B_r^0(r,z) = 0 , \tag{3}$$

in the beam interior where $r < R_b << k_0^{-1}$.

Assuming a tenuous electron beam with negligibly small equilibrium self fields, then the electron motion in the longitudinal wiggler field specified by Eq. (3) is characterized by four single-particle constants of the motion. These are:

$$p_z \ ,$$

$$p_\perp^2 = p_r^2 + p_\theta^2 \ ,$$

$$\gamma mc^2 = (m^2c^4 + c^2p_\perp^2 + c^2p_z^2)^{1/2} \ , \tag{4}$$

$$P_\theta = r\left(p_\theta - \frac{e}{c} A_\theta^0(r,z)\right) \ ,$$

where p_z is the axial momentum, $p_\perp$ is the perpendicular momentum, γmc^2 is the electron energy, and

$$A_\theta^0(r,z) = \frac{1}{2} rB_0\left(1 + \frac{\delta B}{B_0} \sin k_0 z\right) \ , \tag{5}$$

is the θ-component of vector potential consistent with Eq. (3). Here, $-e$ is the electron charge, m is the electron rest mass, and c is the speed of light in vacuo. Note that γmc^2 = const. can be constructed from the constants of the motion p_z and $p_\perp^2$, which are independently conserved.

It is important to keep in mind that the validity of the single-particle constants of the motion in Eq. (4) assumes that $k_0^2r^2 << 1$, $\delta B/B_0 < 1$, and that the oscillatory radial magnetic field $B_r^0 \simeq -(\delta B/2)k_0 r \cos k_0 z$ can be approximated by $B_r^0 = 0$ [Eq. (3)]. To determine the range of

validity of this approximation, we have also calculated[1] (in an iterative sense) the leading-order corrections to the longitudinal and transverse orbits, treating the magnetic force $(-e/c)\underset{\sim}{v}\times B_r^0 \hat{\underset{\sim}{e}}_r$ as a small correction.

B. Beam Equilibrium Properties

The TE-mode stability analysis in Sec. III is carried out for perturbations about the self-consistent equilibrium distribution[36]

$$f_b^0(\underset{\sim}{x},\underset{\sim}{p}) = \frac{\hat{n}_b}{\pi}\,\delta(p_\perp^2 - 2\gamma_b m\omega_b P_\theta - 2\gamma_b m\hat{T}_{\perp b})\delta(p_z - \gamma_b m V_b)\ , \tag{6}$$

where $\hat{n}_b$, $\hat{T}_{\perp b}$, ω_b and V_b are constants, $\gamma_b mc^2$ = const. is the characteristic energy of a beam electron, and $\hat{V}_{\perp b}$ is defined by $\hat{V}_{\perp b} = (2\hat{T}_{\perp b}/\gamma_b m)^{1/2}$. Making use of Eq. (4), it is readily shown that

$$\begin{aligned} p_\perp^2 - 2\gamma_b m\omega_b P_\theta &= p_r^2 + (p_\theta - \gamma_b m\omega_b r)^2 \\ &\quad + \gamma_b^2 m^2 r^2 \omega_b \left\{\omega_{cb}\left(1 + \frac{\delta B}{B_0}\sin k_0 z\right) - \omega_b\right\}\ , \end{aligned} \tag{7}$$

where $\omega_{cb} = eB_0/\gamma_b mc$ is the relativistic cyclotron frequency. From Eqs. (6) and (7), it readily follows that the average axial and azimuthal momentum of the beam electrons are given by

$$\begin{aligned} \langle p_z\rangle &\equiv \frac{\int d^3p\ p_z f_b^0}{\int d^3p\ f_b^0} = \gamma_b m V_b\ , \\ \langle p_\theta\rangle &\equiv \frac{\int d^3p\ p_\theta f_b^0}{\int d^3p\ f_b^0} = \gamma_b m\omega_b r. \end{aligned} \tag{8}$$

Moreover, it can be shown from Eqs. (6) and (7) that $f_b^0(\underset{\sim}{x},\underset{\sim}{p})$ corres-

ponds to a sharp-boundary equilibrium[36] with density profile $n_b^0(\underset{\sim}{x}) = \int d^3p\, f_b^0$ given by

$$n_b^0(r,z) = \begin{cases} \hat{n}_b = \text{const.}, & 0 < r < R_b(z) , \\ 0 , & r > R_b(z) . \end{cases} \tag{9}$$

Here, the radial boundary $R_b(z)$ of the electron beam is defined by

$$R_b^2(z) = \frac{\hat{V}_{\perp b}^2}{\omega_b\{\omega_{cb}[1+(\delta B/B_0)\sin k_0 z]-\omega_b\}} , \tag{10}$$

where $\hat{V}_{\perp b}^2 = 2\hat{T}_{\perp b}/\gamma_b m$. From Eq. (10), ω_b is required to be in the range

$$0 < \omega_b < \omega_{cb}[1-\delta B/B_0] \tag{11}$$

for a radially confined equilibrium to exist. Moreover, the maximum beam radius $[R_b]_{MAX}$ occurs for $k_0 z=(2n+1)\pi/2$, $n=\pm 1, \pm 2, \ldots$ Introducing the effective thermal Larmor radius $r_{Lb} = \hat{V}_{\perp b}/\omega_{cb}$, the condition $k_0^2[R_b]_{MAX}^2 \ll 1$ can readily be expressed as

$$k_0^2 r_{Lb}^2 \ll \frac{\omega_b}{\omega_{cb}}\left(1 - \frac{\delta B}{B_0} - \frac{\omega_b}{\omega_{cb}}\right) . \tag{12}$$

The stability analysis in Sec. III is carried out for the case where the beam rotation is slow with

$$\omega_b \ll \omega_{cb} , \tag{13}$$

and the wiggler amplitude is small with $\delta B/B_0 \ll 1$. In this case,

the axial modulation of the beam radius in Eq. (10) is very weak, and $R_b(z)$ can be approximated by the constant value

$$R_b(z) \simeq \hat{R}_b = \left(\frac{\hat{V}_{\perp b}^2}{\omega_b \omega_{cb}}\right)^{1/2} . \tag{14}$$

Moreover, consistent with Eqs. (13) and (14), it is valid to approximate $P_\theta \simeq -\gamma_b m\omega_{cb} r^2/2$ in Eq. (7), which gives

$$\begin{aligned} p_\perp^2 - 2\gamma_b m\omega_b P_\theta - 2\gamma_b m\hat{T}_{\perp b} \\ = p_\perp^2 - (\gamma_b m\hat{V}_{\perp b})^2(1-r^2/\hat{R}_b^2) \end{aligned} \tag{15}$$

for $\omega_b << \omega_{cb}$ and $\delta B << B_0$. The equilibrium distribution function in Eq. (6) can then be expressed to the required accuracy as

$$f_b^0(\underset{\sim}{x},\underset{\sim}{p}) = \frac{\hat{n}_b}{\pi}\,\delta[p_\perp^2 - (\gamma_b m\hat{V}_{\perp b})^2(1-r^2/\hat{R}_b^2)]\delta(p_z-\gamma_b mV_b) , \tag{16}$$

where $p_\perp^2 = p_r^2+p_\theta^2$. Equation (16) readily gives the rectangluar density profile in Eq. (9) with constant beam radius equal to $\hat{R}_b$. Note from Eq. (16) that the equilibrium distribution function has an inverted population[1] in $p_\perp$ with $f_b^0 = \text{const.} \times \delta[p_\perp^2 - p_{\perp 0}^2(r)]\delta(p_z-\gamma_b mV_b)$, where $p_{\perp 0}^2(r) = (\gamma_b m\hat{V}_{\perp b})^2(1-r^2/\hat{R}_b^2)$.

C. Particle Trajectories in the Equilibrium Fields

The orbit equations for an electron moving in the axial magnetic field $B_z^0(z) = B_0+\delta B\sin k_0 z$ described by Eq. (3) are given by $dp_x'/dt' = -(e/c)v_y'B_z^0(z')$, $dp_y'/dt' = (e/c)v_x'B_z^0(z')$ and $dp_z'/dt'=0$, where $\underset{\sim}{p}(t') = \gamma m\underset{\sim}{v}'(t')$ and $\gamma = (1+\underset{\sim}{p}'^2/m^2c^2)^{1/2} = \text{const.}$ The axial trajectory

(z',p_z') that passes through the phase space point (z,p_z) at time $t'=t$ is given by

$$p_z' = p_z \ , \quad z' = z + v_z\tau \ , \tag{17}$$

where $\tau = t'-t$ and $v_z=p_z/\gamma m$=const. is the axial velocity. Defining $v_+'(t)=v_x'(t')+iv_y'(t')$ and making use of Eq. (17), it is straightforward to show that $v_+'(t')$ satisfies

$$\frac{d}{dt'} v_+' = i\omega_c \left(1 + \frac{\delta B}{B_0} \sin(k_0z+k_0v_z\tau)\right) v_+' \ , \tag{18}$$

where $\omega_c = eB_0/\gamma mc$ is the relativistic cylotron frequency for electron motion in the average field B_0. Integrating Eq. (18) with respect to t' and enforcing $v_+'(t'=t)=v_x+iv_y=v_\perp\exp(i\phi)$, where $(v_x,v_y) = (v_\perp\cos\phi, v_\perp\sin\phi)$ is the perpendicular velocity at time $t'=t$, gives[1]

$$v_+'(t') = v_\perp \exp\left(i\phi+i\omega_c\tau + i\omega_c \frac{\delta B}{B_0} \frac{\cos k_0z-\cos(k_0z+k_0v_z\tau)}{k_0v_z}\right). \tag{19}$$

From Eq. (19), we note that $|v_+'(t')|$ = const., as expected. However, the individual transverse velocity components, $v_x'(t')$ and $v_y'(t')$, can be strongly modulated as a function of z and t' by the longitudinal wiggler field $\delta B\sin k_0z$. Depending on the size of $\delta B/B_0$, this can lead to a significant enhancement of radiation emission relative to the case where $\delta B=0$.

For future reference, it is convenient to Fourier decompose the k_0z dependence in Eq. (19), making use of the Bessel function identity

$$\exp(ib\ \cos\alpha) = \sum_{m=-\infty}^{\infty} J_m(b)\exp(-im\alpha+im\pi/2) \ ,$$

where $J_m(b)$ is the Bessel function of the first kind of order m. This gives

$$v_+'(t') = v_\perp \exp(i\phi) \sum_{m,n} J_m\left(\frac{\omega_c}{k_0 v_z}\frac{\delta B}{B_0}\right) J_n\left(\frac{\omega_c}{k_0 v_z}\frac{\delta B}{B_0}\right) (i)^{n-m}$$
$$\times \exp[i(\omega_c\tau+mk_0v_z\tau)]\exp[i(m-n)k_0z] \ , \qquad (20)$$

where $\sum_{m,n}$ denotes $\sum_{m=-\infty}^{\infty}\sum_{n=-\infty}^{\infty}$. From Eq. (20), for $(\omega_c/k_0v_z)(\delta B/B_0)$ of order unity, we note that the temporal modulation of the perpendicular velocity can be strong at harmonics of $k_0v_z \simeq k_0V_b$. Finally, when Eq. (20) is integrated with respect to t' to determine the transverse particle orbit $x'(t')+iy(t')$, we note that there are resonant contributions proportional to $(\omega_c+mk_0v_z)^{-1}$. In this regard, the present analysis assumes that $v_z \simeq V_b$ is sufficiently far removed from cyclotron resonance (with $\omega_c+mk_0V_b \neq 0$) that the particle orbits do not exhibit large (secular) transverse excursions.[1]

III. TE-MODE STABILITY PROPERTIES

A. Linearized Vlasov-Maxwell Equations

For the equilibrium configuration discussed in Sec. II, we now make use of the linearized Vlasov-Maxwell equations to investigate stability properties for electromagnetic perturbations with TE-mode polarization. It is assumed that a conducting wall is located at radius $r = R_c > \hat{R}_b$. Moreover, perturbed quantities are expressed as

$$\delta\psi(\underset{\sim}{x},t) = \delta\hat{\psi}(\underset{\sim}{x})\exp(-i\omega t) \ ,$$

where $\mathrm{Im}\omega>0$ corresponds to instability. We consider azimuthally symmetric ($\partial/\partial\theta=0$) TE-mode perturbations with electromagnetic field components

$$\delta\hat{\underset{\sim}{E}}(\underset{\sim}{x}) = \delta\hat{E}_\theta(r,z)\hat{\underset{\sim}{e}}_\theta \ ,$$

$$\delta\hat{\underset{\sim}{B}}(\underset{\sim}{x}) = \delta\hat{B}_r(r,z)\hat{\underset{\sim}{e}}_r + \delta\hat{B}_z(r,z)\hat{\underset{\sim}{e}}_z \ , \tag{21}$$

where $(\hat{\underset{\sim}{e}}_r,\hat{\underset{\sim}{e}}_\theta,\hat{\underset{\sim}{e}}_z)$ are unit vectors in the (r,θ,z) directions. The Maxwell equations for $\delta\hat{\underset{\sim}{E}}$ and $\delta\hat{\underset{\sim}{B}}$ are given by

$$\nabla\times\delta\hat{\underset{\sim}{E}} = \frac{i\omega}{c}\,\delta\hat{\underset{\sim}{B}} \ , \tag{22}$$

$$\nabla\times\delta\hat{\underset{\sim}{B}} = -\frac{4\pi e}{c}\int d^3p\ \underset{\sim}{v}\,\delta\hat{f}_b - \frac{i\omega}{c}\,\delta\underset{\sim}{E} \ , \tag{23}$$

where $\delta\hat{\underset{\sim}{J}}(\underset{\sim}{x}) = -e\int d^3p\ \underset{\sim}{v}\,\delta\hat{f}_b$ is the perturbed current density, and $\delta\hat{f}_b(r,z,\underset{\sim}{p})$ is the perturbed distribution function. From Eqs. (21) and (22), $\delta\hat{B}_z(r,z)$

and $\delta\hat{B}_r(r,z)$ are related to $\delta\hat{E}_\theta(r,z)$ by

$$\delta\hat{B}_z = -\frac{ic}{\omega r}\frac{\partial}{\partial r}(r\delta\hat{E}_\theta) \ , \qquad \delta\hat{B}_r = \frac{ic}{\omega}\frac{\partial}{\partial z}\delta\hat{E}_\theta \ . \tag{24}$$

Moreover, substituting Eq. (22) into Eq. (23) and taking the θ-component gives

$$\left(\frac{\omega^2}{c^2} + \frac{1}{r}\frac{\partial}{\partial r}\, r\, \frac{\partial}{\partial r} - \frac{1}{r^2} + \frac{\partial^2}{\partial z^2}\right)\delta\hat{E}_\theta(r,z) = \frac{4\pi i\omega e}{c^2}\int d^3p\ v_\theta\ \delta\hat{f}_b(r,z,\underset{\sim}{p}) \ , \tag{25}$$

which relates $\delta\hat{E}_\theta(r,z)$ to the perturbed azimuthal current density $\delta\hat{J}_\theta(r,z) = -e\int d^3p\ v_\theta\ \delta\hat{f}_b$.

Making use of the method of chracteristics, the linearized Vlasov equation for $\delta f_b(r,z,\underset{\sim}{p},t) = \delta\hat{f}_b(r,z,\underset{\sim}{p})\exp(-i\omega t)$ can be integrated to give

$$\delta\hat{f}_b(r,z,\underset{\sim}{p}) = e\int_{-\infty}^{t} dt'\exp[-i\omega(t'-t)] \times \left(\delta\underset{\sim}{\hat{E}}(\underset{\sim}{x}') + \frac{\underset{\sim}{v}'\times\delta\underset{\sim}{\hat{B}}(\underset{\sim}{x}')}{c}\right)\cdot\left(\frac{\partial}{\partial\underset{\sim}{p}}\, f_b^0\right)_{(\underset{\sim}{x}',\underset{\sim}{p}')} \ , \tag{26}$$

where $(\underset{\sim}{x}',\underset{\sim}{p}')$ are the particle trajectories in the equilibrium field configuration (Sec. II.C) that pass through the phase space point $(\underset{\sim}{x},\underset{\sim}{p})$ at time $t'=t$, and $f_b^0(\underset{\sim}{x},\underset{\sim}{p})$ is the equilibrium distribution function. We first simplify Eq. (26) for the general class of self-consistent Vlasov equilibria (Sec. II.B),

$$f_b^0(\underset{\sim}{x},\underset{\sim}{p}) = f_b^0(p_\perp^2 - 2\gamma_b m\omega_b P_\theta, p_z), \tag{27}$$

where the perturbed electromagnetic fields have the components shown in Eq. (21). After some straightforward algebra, the perturbed distribution function can be expressed as

$$\begin{aligned}\delta\hat{f}_b(r,z,\underset{\sim}{p}) = 2e\frac{\partial f_b^0}{\partial p_\perp^2}\int_{-\infty}^{0} d\tau\ \exp(-i\omega\tau)\ \Big\{&[\delta\hat{E}_\theta(r',z') + \frac{1}{c}v_z'\delta\hat{B}_r(r',z')] \\ &\times (p_\theta' - \gamma_b m\omega_b r') + \gamma_b m\omega_b r'\frac{1}{c}v_r'\delta\hat{B}_z(r',z')\Big\} \\ - e\frac{\partial f_b^0}{\partial p_z}\int_{-\infty}^{0} d\tau\ \exp(-i\omega\tau)\frac{1}{c}v_\theta'&\delta\hat{B}_r(r',z')\ ,\end{aligned} \tag{28}$$

where $\tau = t' - t$. In obtaining Eq. (28), use has been made of the fact that $\partial f_b^0/\partial p_\perp^2$ and $\partial f_b^0/\partial p_z$ are constant (independent of t') along a particle trajectory in the equilibrium field configuration. Moreover, from Sec. II.B, $v_z' = v_z = p_z/\gamma m$ and $\gamma' = \gamma = (1+\underset{\sim}{p}^2/m^2c^2)^{1/2}$ are independent of t' in Eq. (28), and the axial orbit is given by $z' = z + v_z\tau$. In addition, the transverse velocities $v_r' = dr'/dt'$ and $v_\theta' = r'd\theta'/dt'$ can be determined from Eq. (19), subject to the boundary conditions $v_r'(t'=t) = v_r$, $v_\theta'(t'=t) = v_\theta$, $r'(t'=t) = r$ and $\theta'(t'=t) = \theta$.

Equation (28) simplifies considerably in the case of very slow beam rotation ($\omega_b << \omega_{cb}$) and weak wiggler field ($\delta B << B_0$) discussed in Sec. II.B. Neglecting the terms proportional to ω_b in Eq. (28), and expressing $\delta\hat{B}_r$ in terms of $\delta\hat{E}_\theta$ [Eq. (24)], we obtain

$$\begin{aligned}\delta\hat{f}_b(r,z,\underset{\sim}{p}) = 2e\frac{\partial f_b^0}{\partial p_\perp^2}\int_{-\infty}^{0} d\tau\ \exp(-i\omega\tau)p_\theta'\delta\hat{E}_\theta(r',z') \\ + \frac{ie}{\gamma m\omega}\left(2p_z\frac{\partial f_b^0}{\partial p_\perp^2} - \frac{\partial f_b^0}{\partial p_z}\right)\int_{-\infty}^{0} d\tau\exp(-i\omega\tau)p_\theta'\frac{\partial}{\partial z'}\hat{\delta E}_\theta(r',z'),\end{aligned} \tag{29}$$

where $z' = z + v_z\tau$. In general, Eq. (29) is to be substituted into Eq. (25) and the resulting equation solved as an eigenvalue equation for $\delta\hat{E}_\theta(r,z)$ and ω.

B. Matrix Dispersion Equation for a Tenuous Beam

For a low-density electron beam, we make use of the fact that the solution for $\delta\hat{E}_\theta(r,z)$ is closely approximated by the vacuum waveguide solution, and solve Eqs. (25) and (29) in an iterative sense. In particular, we express[37-39]

$$\delta\hat{E}_\theta(r,z) = \delta\tilde{E}_\theta(z)J_1(\alpha_{0\ell}r/R_c) \ , \tag{30}$$

where $\alpha_{0\ell}$ is the ℓ'th zero of $J_1(\alpha_{0\ell}) = 0$, and $\delta\hat{E}_\theta(r=R_c,z) = 0$ at the conducting wall. Here, $J_n(x)$ is the Bessel function of the first kind of order n. Taylor expanding the z'-dependence of $\delta\hat{E}_\theta(r',z')$ in Eq. (29) according to

$$\delta\tilde{E}_\theta(z') = \sum_{k=-\infty}^{\infty} \delta\tilde{E}_\theta(k)\exp(ikz+ikv_z\tau) \ , \tag{31}$$

where $k=2\pi n/L$ and L is the periodicity length in the z-direction, we readily find

$$\delta\hat{f}_b(r,z,p) = e\sum_k \delta\tilde{E}_\theta(k)\exp(ikz)\left\{2\left(1-\frac{kv_z}{\omega}\right)\frac{\partial f_b^0}{\partial p_\perp^2} + \frac{k}{\gamma m\omega}\frac{\partial f_b^0}{\partial p_z}\right\} \times \int_{-\infty}^{0} d\tau\ \exp(-i\omega\tau+ikv_z\tau)p_\theta' J_1(\alpha_{0\ell}r'/R_c) \ . \tag{32}$$

We substitute Eqs. (30) and (32) into Eq. (25), make use of

$\{r^{-1}(\partial/\partial r)[r(\partial/\partial r)]-r^{-2}\}J_1(\alpha_{0\ell}r/R_c) = -(\alpha_{0\ell}^2/R_c^2)J_1(\alpha_{0\ell}r/R_c)$, and operate with $\int_0^{R_c} dr\ r\ J_1(\alpha_{0\ell}r/R_c)\ldots$. This gives

$$\left(\frac{\omega^2}{c^2} - \frac{\alpha_{0\ell}^2}{R_c^2} + \frac{\partial^2}{\partial z^2}\right)\delta\tilde{E}_\theta(z)$$

$$= \frac{(4\pi e^2 i\omega/c^2)}{[R_c^2 J_2^2(\alpha_{0\ell})/2]}\int_0^{R_c} dr\ r\ J_1\left(\frac{\alpha_{0\ell}r}{R_c}\right)\sum_k \delta\tilde{E}_\theta(k)\exp(ikz)$$

$$\times \int d^3p\ v_\theta \left\{2\left(1 - \frac{kv_z}{\omega}\right)\frac{\partial f_b^0}{\partial p_\perp^2} + \frac{k}{\gamma m\omega}\frac{\partial f_b^0}{\partial p_z}\right\} \tag{33}$$

$$\times \int_{-\infty}^{0} d\tau\ \exp(-i\omega\tau+ikv_z\tau)p_\theta' J_1(\alpha_{0\ell}r'/R_c)\ ,$$

where use has been made of $\int_0^{R_c} dr\ r\ J_1^2(\alpha_{0\ell}r/R_c) = (R_c^2/2)J_2^2(\alpha_{0\ell})$.

We now evaluate the orbit integral

$$I = \int_{-\infty}^{0} d\tau\ \exp(-i\omega\tau+ikv_z\tau)p_\theta' J_1(\alpha_{0\ell}r'/R_c)\ . \tag{34}$$

The azimithal momentum p_θ' is expressed as $p_\theta' = p_\perp \sin(\phi'-\theta')$, where $p_\perp' = p_\perp = \gamma m v_\perp$ is constant (independent of t') for the equilibrium field configuration described in Sec. II. Equation (34) then becomes

$$I = p_\perp \int_{-\infty}^{0} d\tau\ \exp(-i\omega\tau+ikv_z\tau)\sin(\phi'-\theta')J_1(\alpha_{0\ell}r'/R_c)\ . \tag{35}$$

To simplify Eq. (35), we specialize to the case of small thermal Larmor radius, $r_{Lb}^2/\hat{R}_b^2 \ll 1$, and approximate the r' and θ' orbits by $(r',\theta') \simeq (r,\theta)$. This is an excellent approximation for a slowly rotating beam with $\omega_b/\omega_{cb} \ll 1$, since $r_{Lb}^2/\hat{R}_b^2 = \hat{V}_{\perp b}^2/\omega_{cb}^2\hat{R}_b^2 = \omega_b/\omega_{cb} \ll 1$ follows from Eq. (14). The orbit integral I in Eq. (35) can then be approximated by

$$I = p_\perp J_1(\alpha_{0\ell} r/R_c) \int_{-\infty}^{0} d\tau \exp(-i\omega\tau + ikv_z\tau)$$

$$\times \frac{1}{2i} \{\exp[i(\phi'-\theta)] - \exp[-i(\phi'-\theta)]\} , \tag{36}$$

where ϕ' is the rapidly oscillating velocity phase defined by [Eq. (19)],

$$\phi' = \phi + \omega_c\tau + \omega_c \frac{\delta B}{B_0}\left(\frac{\cos k_0 z - \cos(k_0 z + k_0 v_z \tau)}{k_0 v_z}\right). \tag{37}$$

We substitute Eq. (37) into Eq. (36), make use of the Bessel function identity in Eq. (20) to expand $\exp(\pm i\phi')$, and then carry out the integration over τ for $\mathrm{Im}\omega > 0$. After some straightforward algebra, this gives

$$I = \frac{p_\perp J_1(\alpha_{0\ell} r/R_c)}{2i} \sum_{n,m} J_n\left(\frac{\omega_c}{k_0 v_z}\frac{\delta B}{B_0}\right) J_m\left(\frac{\omega_c}{k_0 v_z}\frac{\delta B}{B_0}\right)$$

$$\times \left\{ \frac{\exp[i(\phi-\theta)]\exp[-i(n-m)k_0 z](i)^{n-m+1}}{\omega-(k+mk_0)v_z-\omega_c} \right.$$

$$\left. - \frac{\exp[-i(\phi-\theta)]\exp[-i(n-m)k_0 z](i)^{-n+m+1}}{\omega-(k+mk_0)v_z+\omega_c} \right\} , \tag{38}$$

where $\omega_c = eB_0/\gamma mc$, $v_z = p_z/\gamma m$ and $\sum_{n,m}$ denotes $\sum_{n=-\infty}^{\infty} \sum_{m=-\infty}^{\infty}$. In the eigenvalue equation (33), we express $\int d^3p = \int_0^{2\pi} d\phi \int_0^{\infty} dp_\perp p_\perp \int_{-\infty}^{\infty} dp_z$ and carry out the required integration over ϕ, making use of $v_\theta = (p_\perp/\gamma m)\sin(\phi-\theta)$ and the fact that $f_b^0 = f_b^0[p_\perp^2 - (\gamma_b m \hat{V}_{\perp b})^2(1-r^2/\hat{R}_b^2), p_z]$ is independent of ϕ to the level of accuracy of Eq. (15). In particular, we readily obtain from Eq. (38)

$$\int_0^{2\pi} d\phi v_\perp \sin(\phi-\theta) I$$

$$= -\frac{2\pi p_\perp^2}{4\gamma mi} J_1(\alpha_{0\ell} r/Rc) \sum_{n,m} J_n\left(\frac{\omega_c}{k_0 v_z}\frac{\delta B}{B_0}\right) J_m\left(\frac{\omega_c}{k_0 v_z}\frac{\delta B}{B_0}\right) \exp[-i(n-m)k_0 z] \tag{39}$$

$$\times \left\{\frac{(i)^{n-m}}{\omega-(k+mk_0)v_z-\omega_c} - \frac{(i)^{-n+m}}{\omega-(k+mk_0)v_z+\omega_c}\right\} .$$

Substituting Eq. (39) into Eq. (33), the eigenvalue equation for $\delta\tilde{E}_\theta(z)$ can be expressed as

$$\left(\frac{\partial^2}{\partial z^2} - \frac{\alpha_{0\ell}^2}{R_c^2} + \frac{\omega^2}{c^2}\right)\delta\tilde{E}_\theta(z)$$

$$= -\sum_k \sum_{m,n} \chi_{m,n}(k,\omega)\delta\tilde{E}_\theta(k) \tag{40}$$

$$\times \exp[i(k+mk_0-nk_0)z] ,$$

where the susceptibility $\chi_{m,n}(k,\omega)$ is defined by

$$\chi_{m,n}(k,\omega) = \frac{1}{4}\frac{(4\pi e^2/c^2)}{[(R_c^2/2)J_2^2(\alpha_{0\ell})]} \int_0^r dr\, r\, J_1^2(\alpha_{0\ell} r/R_c)$$

$$\times \int d^3p\, J_m\left(\frac{\omega_c}{k_0 v_z}\frac{\delta B}{B_0}\right) J_n\left(\frac{\omega_c}{k_0 v_z}\frac{\delta B}{B_0}\right)$$

$$\times v_\perp^2\left[\frac{\gamma m\omega}{p_\perp}\frac{\partial f_b^0}{\partial p_\perp} + k\left(\frac{\partial f_b^0}{\partial p_z} - \frac{p_z}{p_\perp}\frac{\partial f_b^0}{\partial p_\perp}\right)\right] \tag{41}$$

$$\times \left\{\frac{(i)^{n-m}}{\omega-(k+mk_0)v_z-\omega_c} - \frac{(i)^{-n+m}}{\omega-(k+mk_0)v_z+\omega_c}\right\} .$$

In Eq. (41), $v_\perp = p_\perp/\gamma m$, $v_z = p_z/\gamma m$, $\omega_c = eB_0/\gamma mc$ and $\int d^3p = 2\pi \int_0^\infty dp_\perp p_\perp \int_{-\infty}^{\infty} dp_z$. Equations (40) and (41) should be compared with Eqs. (22) and (23) of Ref. 1. The major difference is that Eqs. (40) and (41) include finite radial beam geometry in a fully self-consistent manner, whereas Ref. 1 assumes an infinite uniform beam in the transverse direction. The effects of finite radial geometry are manifest through the occurrence of the effective perpendicular wavenumber $\alpha_{0\ell}$ on the left-hand side of Eq. (40), as well as the r-integration over $J_1^2(\alpha_{0\ell} r/R_c)$ and the r-dependence of the equilibrium distribution function f_b^0 in Eq. (41) [see Eqs. (15) and (16)]. Fourier decomposing the left-hand side of Eq. (40) with respect to z, and changing the k-summation variable on the right-hand side of Eq. (40) from $k+mk_0-nk_0 \to k$ gives

$$\sum_k \left(\frac{\omega^2}{c^2} - \frac{\alpha_{0\ell}^2}{R_c^2} - k^2\right) \delta\tilde{E}_\theta(k)\exp(ikz) + \sum_k \sum_{m,n} \chi_{m,n}(k+nk_0-mk_0,\omega)\delta\tilde{E}_\theta(k+nk_0-mk_0)\exp(ikz) = 0 \ . \tag{42}$$

Equation (42) gives the final dispersion equation

$$D_0(k,\omega)\delta\tilde{E}_\theta(k) + \sum_{N\neq 0} \chi_N(k+Nk_0,\omega)\delta\tilde{E}_\theta(k+Nk_0) = 0 \ , \tag{43}$$

where $\sum_{N\neq 0} = \sum_{N=-\infty}^{-1} + \sum_{N=1}^{\infty}$, and D_0 and χ_N are defined by

$$D_0(k,\omega) \equiv \left[\frac{\omega^2}{c^2} - k^2 - \frac{\alpha_{0\ell}^2}{R_c^2}\right] + \chi_0(k,\omega) \ , \tag{44}$$

and

$$\chi_N(k+Nk_0,\omega) \equiv \sum_{n=-\infty}^{\infty} \chi_{n-N,n}(k+Nk_0,\omega) \ . \tag{45}$$

The dispersion equation (43) can be used to investigate stability properties for a wide range of system parameters. To lowest-order, the stability analysis in Sec. IV is based on a diagonal approximation to Eq. (43), i.e.,

$$D_0(k,\omega) = 0 \ , \tag{46}$$

which neglects the coupling of $\delta\tilde{E}_\theta(k)$ to the higher harmonic dependence in $\delta E_\theta(k+Nk_0)$ for $N\neq 0$. Making use of Eqs. (44) and (45), the approximate dispersion relation (46) reduces to

$$\left(\frac{\omega^2}{c^2} - k^2 - \frac{\alpha_{0\ell}^2}{R_c^2}\right) + \sum_{n=-\infty}^{\infty} \chi_{n,n}(k,\omega) = 0 \ , \tag{47}$$

which is analyzed in Sec. IV.

C. Susceptibility for a Nonuniform Beam

We now evaluate the susceptibility $\chi_{m,n}(k,\omega)$ defined in Eq. (41) for the specific choice of radially nonuniform beam equilibrium in Eq. (16). The evaluation of $\chi_{m,n}(k,\omega)$ proceeds in a manner similar to Ref. 1 with the important difference that the $p_\perp$- and p_z-integrations in Eq. (41) select spatially nonuniform values of $p_\perp$ and γmc^2 for the choice of f_b^0 in Eq. (16). In this regard, it is convenient to define

$$\hat{p}_{\perp b} = \gamma_b m \hat{V}_{\perp b} \ ,$$

$$p_{zb} = \gamma_b m V_b \ , \tag{48}$$

$$\gamma_b = (1+p_{zb}^2/m^2c^2)^{1/2} = (1-V_b^2/c^2)^{-1/2} \ .$$

(Heretofore, γ_b has been a convenient scale factor, with $\gamma_b mc^2$ a measure to the characteristic electron energy.) It is clear from Eq. (16) that the delta-function form of f_b^0 selects the values of perpendicular momentum $p_\perp = p_{\perp 0}(r)$, total energy $\gamma mc^2 = \gamma_0(r)mc^2$, perpendicular velocity $v_\perp = p_\perp/\gamma m = V_{\perp 0}(r)$, and axial velocity $v_z = p_z/\gamma m = V_{b0}(r)$, where

$$\begin{aligned}
p_{\perp 0}^2(r) &\equiv \hat{p}_{\perp b}^2\left(1 - \frac{r^2}{\hat{R}_b^2}\right) \ , \\
\gamma_0(r) &\equiv \gamma_b\left[1 + \frac{\hat{V}_{\perp b}^2}{c^2}\left(1 - \frac{r^2}{\hat{R}_b^2}\right)\right]^{1/2} \ , \\
V_{\perp 0}(r) &\equiv \frac{\gamma_b}{\gamma_0(r)}\,\hat{V}_{\perp b}(1-r^2/\hat{R}_b^2)^{1/2} \ , \\
V_{b0}(r) &\equiv V_b\,\frac{\gamma_b}{\gamma_0(r)} \ ,
\end{aligned} \tag{49}$$

for $0 < r < \hat{R}_b$. Note from Eq. (49) that $p_{\perp 0}(r)$ and $V_{\perp 0}(r)$ are highly nonuniform across the beam cross-section, assuming maximum values on the axis of the beam (r=0), and minimum values of zero at the edge of the beam ($r=\hat{R}_b$). On the other hand, for $\hat{V}_{\perp b}^2/c^2 << 1$, the variation of $\gamma_0(r)$ and $V_{b0}(r)$ is relatively weak over the beam cross section.

Substituting Eq. (16) into Eq. (41) and carrying out the integrations over $p_\perp$ and p_z, we find after some straightforward but

tedious algebra that $\chi_{m,n}(k,\omega)$ can be expressed as

$$\chi_{m,n}(k,\omega) = -\frac{1}{4}\frac{\omega_{pb}^2}{c^2}\frac{1}{[(R_c^2/2)J_2^2(\alpha_{0\ell})]}\int_0^{\hat{R}_b} dr\, r\, J_1^2\left(\alpha_{0\ell}\frac{r}{R_c}\right)$$

$$\times J_m\left(\frac{\omega_{cb}}{k_0 V_b}\frac{\delta B}{B_0}\right) J_n\left(\frac{\omega_{cb}}{k_0 V_b}\frac{\delta B}{B_0}\right)\frac{\gamma_b}{\gamma_0}$$

$$\times \left\{\left(\frac{(i)^{n-m}}{\omega-(k+nk_0)V_b\gamma_b/\gamma_0-\omega_{cb}\gamma_b/\gamma_0}\left[2\left[\omega-(k+nk_0-mk_0)V_b\frac{\gamma_b}{\gamma_0}\right]\right.\right.\right.$$

$$+\frac{V_{\perp 0}^2(r)}{c^2}\frac{(k+nk_0-mk_0)c^2}{V_b}\frac{\gamma_b}{\gamma_0}\varepsilon_{m,n} \qquad (50)$$

$$\left.\left.\left.-\frac{V_{\perp 0}^2(r)}{c^2}\frac{1}{\omega-(k+nk_0)V_b\gamma_b/\gamma_0-\omega_{cb}\gamma_b/\gamma_0}\left[\omega^2-(k+nk_0-mk_0)(k+nk_0)c^2\right]\right]\right)$$

$$\left.+\left(\omega_{cb}\rightarrow-\omega_{cb}\right)\right\},$$

where $\omega_{pb}^2 = 4\pi\hat{n}_b e^2/\gamma_b m$, $\omega_{cb} = eB_0/\gamma_b mc$, and $\gamma_0(r)$ and $V_{\perp 0}(r)$ are defined in Eq. (49). Here, $\varepsilon_{m,n}$ is defined by[1]

$$\varepsilon_{m,n} = \left\{p_z\frac{\partial}{\partial p_z}\,\ell n\left[J_n\left(\frac{e\delta B}{k_0 c p_z}\right)\,J_m\left(\frac{e\delta B}{k_0 c p_z}\right)\right]\right\}_{p_z=\gamma_b m V_b} \qquad (51)$$

The r-dependence of the integrand in Eq. (50) is generally quite complicated. For present purposes, we assume $\hat{V}_{\perp b}^2/c^2 \ll 1$ and approximate $\gamma_0(r) \simeq \gamma_b$ in Eq. (50). This gives the approximate result

$$\chi_{m,n}(k,\omega) = -\frac{1}{4}\frac{\omega_{pb}^2}{c^2}\frac{1}{[(R_c^2/2)J_2^2(\alpha_{0\ell})]}\int_0^{\hat{R}_b} dr\ r\ J_1^2\left(\alpha_{0\ell}\frac{r}{R_c}\right)$$

$$\times J_m\left(\frac{\omega_{cb}}{k_0 V_b}\frac{\delta B}{B_0}\right) J_n\left(\frac{\omega_{cb}}{k_0 V_b}\frac{\delta B}{B_0}\right)$$

$$\times \left\{\left(\frac{(i)^{n-m}}{\omega-(k+nk_0)V_b-\omega_{cb}}\left[2[\omega-(k+nk_0-mk_0)V_b]\right.\right.\right.$$

$$+\frac{\hat{V}_{\perp b}^2}{c^2}\left(1-\frac{r^2}{\hat{R}_b^2}\right)\frac{(k+nk_0-mk_0)c^2}{V_b}\varepsilon_{m,n} \qquad (52)$$

$$\left.\left.\left.-\frac{\hat{V}_{\perp b}^2}{c^2}\left(1-\frac{r^2}{\hat{R}_b^2}\right)\frac{[\omega^2-(k+nk_0-mk_0)(k+nk_0)c^2]}{\omega-(k+nk_0)V_b-\omega_{cb}}\right]\right)\right.$$

$$\left.+\left(\omega_{cb}\to-\omega_{cb}\right)\right\}\ .$$

In Eq. (52), the r-dependence of the integrand is of the form $rJ_1^2(\alpha_{0\ell}r/R_c)$ and $rJ_1^2(\alpha_{0\ell}r/R_c)(1-r^2/\hat{R}_b^2)$. We introduce the geometric factors g_1 and g_2 defined by

$$g_1 = \frac{1}{[(R_c^2/2)J_2^2(\alpha_{0\ell})]}\int_0^{\hat{R}_b} dr\ r\ J_1^2\left(\alpha_{0\ell}\frac{r}{R_c}\right)$$

$$= \frac{\hat{R}_b^2}{R_c^2 J_2^2(\alpha_{0\ell})}\left[J_1'^2\left(\alpha_{0\ell}\frac{\hat{R}_b}{R_c}\right)+\left(1-\frac{R_c^2}{\alpha_{0\ell}^2\hat{R}_b^2}\right)J_1^2\left(\alpha_{0\ell}\frac{\hat{R}_b}{R_c}\right)\right]\ , \qquad (53)$$

and

$$g_2 = \frac{1}{[(R_c^2/2)J_2^2(\alpha_{0\ell})]}\int_0^{\hat{R}_b} dr\ r\left(1-\frac{r^2}{\hat{R}_b^2}\right)J_1^2\left(\alpha_{0\ell}\frac{r}{R_c}\right)$$

$$= \frac{2\hat{R}_b^2}{3R_c^2 J_2^2(\alpha_{0\ell})}\left[J_0^2\left(\alpha_{0\ell}\frac{\hat{R}_b}{R_c}\right)+J_1^2\left(\alpha_{0\ell}\frac{\hat{R}_b}{R_c}\right)\left(1-\frac{2R_c^2}{\alpha_{0\ell}^2\hat{R}_b^2}\right)\right. \qquad (54)$$

$$\left.-\frac{R_c}{\alpha_{0\ell}\hat{R}_b}J_0\left(\alpha_{0\ell}\frac{\hat{R}_b}{R_c}\right)J_1\left(\alpha_{0\ell}\frac{\hat{R}_b}{R_c}\right)\right]\ .$$

Note from Eq. (53) that $g_1=1$ for a uniform density beam filling the waveguide ($\hat{R}_b/R_c=1$). On the other hand, for $\hat{R}_b=R_c$, it follows from Eq. (54) that $g_2 = (2/3)$. Figure 2 shows plots of the geometric factors g_1 and g_2 versus $\hat{R}_b/R_c$ for several values of ℓ. Note that g_1 and g_2 increase monotonically for increasing $\hat{R}_b/R_c$.

Substituting Eqs. (53) and (54) into Eq. (52), we can simplify the expression for $\chi_{m,n}(k,\omega)$ for general values of m and n. In the approximate dispersion relation (47), however, only the diagonal terms are retained. For m=n, Eqs. (52) - (54) give for the susceptibility

$$\chi_{n,n}(k,\omega) = -\frac{1}{4}\frac{\omega_{pb}^2}{c^2} J_n^2\left(\frac{\omega_{cb}}{k_0 V_b}\frac{\delta B}{B_0}\right) \times \left\{\left(\frac{g_1 f_1(\omega)}{[\omega-(k+nk_0)V_b-\omega_{cb}]} - \frac{\hat{V}_{\perp b}^2}{c^2}\frac{g_2 f_2(\omega)}{[\omega-(k+nk_0)V_b-\omega_{cb}]^2}\right) + \left(\omega_{cb} \to -\omega_{cb}\right)\right\} . \tag{55}$$

Here, $\omega_{pb}^2 = 4\pi\hat{n}_b e^2/\gamma_b m$, $\omega_{cb} = eB_0/\gamma_b mc$, g_1 and g_2 are defined in Eqs. (53) and (54), and $f_1(\omega)$ and $f_2(\omega)$ are defined by (for m=n)

$$f_1(\omega) = 2(\omega-kV_b) + \frac{\hat{V}_{\perp b}^2}{c^2}\frac{g_2}{g_1}\frac{kc^2}{V_b}\varepsilon_{n,n} , \tag{56}$$

$$f_2(\omega) = \omega^2 - k(k+nk_0)c^2 . \tag{57}$$

In overall form, Eq. (56) is similar to the result obtained in Ref. 1 for the case of a uniform beam with infinite cross section. There are important differences, however, associated with the dependence of $\chi_{n,n}(k,\omega)$ on the geometric factors g_1 and g_2.

IV. ANALYSIS OF DISPERSION RELATION

A. Approximate Dispersion Relation

Making use of the expression for $\chi_{n,n}(k,\omega)$ in Eq. (55), the approximate dispersion relation (47) for a tenuous beam can be expressed as

$$\left(\frac{\omega^2}{c^2} - k^2 - \frac{\alpha_{0\ell}^2}{R_c^2}\right) = \frac{1}{4}\frac{\omega_{pb}^2}{c^2}\sum_{n=-\infty}^{\infty} J_n^2\left(\frac{\omega_{cb}}{k_0 V_b}\frac{\delta B}{B_0}\right)$$
$$\times \left\{\left(\frac{g_1 f_1(\omega)}{[\omega-(k+nk_0)V_b-\omega_{cb}]} - \frac{\hat{V}_{\perp b}^2}{c^2}\frac{g_2 f_2(\omega)}{[\omega-(k+nk_0)V_b-\omega_{cb}]^2}\right)\right. \tag{58}$$
$$\left. + \left(\omega_{cb} \to -\omega_{cb}\right)\right\} .$$

The dispersion relation (58) clearly has a very rich harmonic content, and Eq. (58) can be solved numerically retaining several terms in the summation over n. For present purposes, we assume that the harmonics in Eq. (58) are well isolated, and investigate stability behavior near cyclotron resonance with polarity

$$\omega - (k+nk_0)V_b \simeq +\omega_{cb} , \tag{59}$$

for a particular choice of harmonic number n. Equation (58) can then be approximated by

$$(\omega^2-c^2k^2-\alpha_{0\ell}^2c^2/R_c^2)[\omega-(k+nk_0)V_b-\omega_{cb}]^2$$
$$= \frac{1}{4}\omega_{pb}^2 J_n^2\left(\frac{\omega_{cb}}{k_0 V_b}\frac{\delta B}{B_0}\right) \tag{60}$$
$$\times \left(g_1 f_1(\omega)[\omega-(k+nk_0)V_b-\omega_{cb}] - \frac{\hat{V}_{\perp b}^2}{c^2} g_2 f_2(\omega)\right) ,$$

where g_1, g_2, f_1, and f_2 are defined in Eqs. (53), (54), (56), and (57). For $\omega \simeq (k+nk_0)V_b+\omega_{cb}$, the first term on the right-hand side of Eq. (60) is negligibly small, and the dispersion relation can be approximated by

$$(\omega^2-c^2k^2-c^2k_{\perp\ell}^2)\left\{[\omega-(k+nk_0)V_b-\omega_{cb}]^2 + \frac{1}{4}\,g_2\omega_{pb}^2\,\frac{\hat{V}_{\perp b}^2}{c^2}\,J_n^2\left(\frac{\omega_{cb}}{k_0V_b}\,\frac{\delta B}{B_0}\right)\right\} = \frac{1}{4}\,g_2\omega_{pb}^2\,\frac{\hat{V}_{\perp b}^2}{c^2}\,J_n^2\left(\frac{\omega_{cb}}{k_0V_b}\,\frac{\delta B}{B_0}\right)(knk_0c^2-k_{\perp\ell}^2c^2)\ . \tag{61}$$

The dispersion relation (60) is solved numerically in Sec. IV.C, and analytic estimates of the instability growth rate are made in Sec. IV.B.

B. Analytic Results

For a tenuous beam with $(\omega_{pb}^2/c^2k^2)(\hat{V}_{\perp b}^2/c^2) \ll 1$, we look for solutions to Eq. (61) near the simultaneous zeroes of

$$\omega = (c^2k^2+c^2k_{\perp\ell}^2)^{1/2}\ , \qquad \omega = (k+nk_0)V_b + \omega_{cb}\ . \tag{62}$$

Here, $k_{\perp\ell} \equiv \alpha_{0\ell}/R_c$ is the effective perpendicular wavenumber, and we have chosen the branch with positive frequency ($\omega>0$) in Eq. (62). Shown in Fig. 3 are plots of ω/ck_0 versus k/k_0 obtained from Eq. (62) for the choice of parameters $k_{\perp\ell}/k_0=9.58$, $V_b/c=0.866$, and $\omega_{cb}/ck_0=4.783$, and several values of the harmonic number n. Denoting the simultaneous

solutions to Eq. (62) by $(\hat{\omega}_n,\hat{k}_n)$, we find for the upshifted frequency and wavenumber

$$\hat{\omega}_n = \gamma_b^2(nk_0V_b+\omega_{cb})\left\{1+\beta_b\left[1-\frac{c^2k_{\perp\ell}^2}{\gamma_b^2(nk_0V_b+\omega_{cb})^2}\right]^{1/2}\right\}, \tag{63}$$

and

$$\hat{k}_n = \gamma_b^2(nk_0V_b+\omega_{cb})\frac{1}{c}\left\{\beta_b+\left[1-\frac{c^2k_{\perp\ell}^2}{\gamma_b^2(nk_0V_b+\omega_{cb})^2}\right]^{1/2}\right\}, \tag{64}$$

where β_b and γ_b are defined by $\beta_b \equiv V_b/c$ and $\gamma_b \equiv (1-\beta_b^2)^{-1/2}$. Note that $(\hat{\omega}_n,\hat{k}_n)$ corresponds to the uppermost intersection points in Fig. 3. Moreover, for $k_{\perp\ell}\to 0$, Eqs. (63) and (64) reduce to the familiar results obtained in Ref. 1 for a uniform density beam with infinite transverse dimension $(\hat{R}_b,R_c\to\infty)$. For solutions to exist, it is clear from Eqs. (63) and (64) that the inequality

$$c^2k_{\perp\ell}^2 = \frac{c^2\alpha_{0\ell}^2}{R_c^2} < \gamma_b^2(nk_0V_b+\omega_{cb})^2 , \tag{65}$$

must be satisfied, which we assume to be the case in the remainder of Sec. IV.

For purposes of making an analytic estimate of the growth rate, we express $\omega=\hat{\omega}_n+\delta\omega$ and $k=\hat{k}_n+\delta k$ in Eq. (61), treating $(\omega_{pb}^2/c^2\hat{k}_n^2)(\hat{V}_{\perp b}^2/c^2)$ as a small parameter. To leading order, this gives

$$\left(\delta\omega - c^2\frac{\hat{k}_n}{\hat{\omega}_n}\delta k\right)\left\{(\delta\omega-V_b\delta k)^2+\frac{1}{4}g_2\omega_{pb}^2\frac{\hat{V}_{\perp b}^2}{c^2}J_n^2\right\} = \frac{1}{8}g_2\omega_{pb}^2\frac{\hat{V}_{\perp b}^2}{c^2}J_n^2\frac{(\hat{k}_nnk_0-k_{\perp\ell}^2)c}{(\hat{k}_n^2+k_{\perp\ell}^2)^{1/2}} , \tag{66}$$

where J_n^2 denotes $J_n^2(\omega_{cb}\delta B/k_0V_bB_0)$, use has been made of $\hat{\omega}_n = (c^2\hat{k}_n^2+c^2k_{\perp\ell}^2)^{1/2}$ [Eq. (62)], and $(\hat{\omega}_n,\hat{k}_n)$ are defined in Eqs. (63) and (64). As a simple analytic estimate of the characteristic maximum growth rate, we consider Eq. (66) for $\delta k=0$. Typically, the J_n^2 contribution on the left-hand side of Eq. (66) makes a small contribution in comparison with the right-hand side, and Eq. (66) can be approximated by (for $\delta k=0$),

$$(\delta\omega)^3 = \Gamma_n^3 \equiv \frac{1}{8}\, g_2\omega_{pb}^2\, \frac{\hat{V}_{\perp b}^2}{c^2}\, J_n^2\, \frac{(\hat{k}_n nk_0-k_{\perp\ell}^2)\,c}{(\hat{k}_n^2+k_{\perp\ell}^2)^{1/2}} \,. \tag{67}$$

For sufficiently short emission wavelength that $\hat{k}_n nk_0 > k_{\perp\ell}^2$, Eq. (67) gives

$$\begin{aligned} \mathrm{Im}\delta\omega &= \frac{\sqrt{3}}{2}\,\Gamma_n = \frac{\sqrt{3}}{4}\left(g_2\omega_{pb}^2 J_n^2\, \frac{\hat{V}_{\perp b}^2}{c^2}\, \frac{(\hat{k}_n nk_0-k_{\perp\ell}^2)\,c}{(\hat{k}_n^2+k_{\perp\ell}^2)^{1/2}}\right)^{1/3}, \\ \mathrm{Re}\delta\omega &= -\frac{1}{2}\,\Gamma_n . \end{aligned} \tag{68}$$

Several points are noteworthy from Eq. (68). First, for a given harmonic number n, the characteristic maximum growth rate $\mathrm{Im}\delta\omega$ defined in Eq. (68) will be largest whenever the argument of J_n corresponds to the first zero of $J_n'(x) = 0$, i.e., when

$$\frac{\omega_{cb}}{k_0V_b}\,\frac{\delta B}{B_0} = \alpha_{n,1} \,, \tag{69}$$

where $\alpha_{n,1}$ is the first zero of $J_n'(x)=0$. Second, since $\mathrm{Im}\delta\omega$ scales as $(\hat{V}_{\perp b}/c)^{2/3}\hat{n}_b^{1/3}$, the growth rate for the longitudinal wiggler FEL can be substantial. Third, the growth rate increases as the geometric factor g_2 is increased (see also Fig. 2). Moreover, the free electron laser instability described by Eq. (61) is inherently

broadband in the sense that many harmonics are unstable, even when $(\omega_{cb}/k_0 V_b)(\delta B/B_0)$ is chosen to maximize emission for a particular value of n [Eq. (69)]. Finally, in the limit of very short emission wavelength with $\hat{k}_n n k_0 >> k_{\perp\ell}^2$, it follows from Eq. (68) that $\mathrm{Im}\delta\omega$ can be approximated by

$$\mathrm{Im}\delta\omega = \frac{\sqrt{3}}{4}\left(g_2 \omega_{pb}^2 n k_0 c J_n^2 \frac{\hat{V}_{\perp b}^2}{c^2}\right)^{1/3} . \tag{70}$$

C. Numerical Results

The dispersion relation (60) is a fourth-order algebraic equation for the complex eigenfrequency ω. Equation (60) has been solved numerically over a wide range of system parameters. In this section, we summarize selected numerical results for $\delta B/B_0 \neq 0$ (longitudinal wiggler free electron laser) and for $\delta B = 0$ (cyclotron maser).

Longitudinal Wiggler Free Electron Laser: Shown in Figs. 4 and 5 are plots of the normalized growth rate $\mathrm{Im}\omega/ck_0$ versus k/k_0 obtained numerically from Eq. (60). The parameters common to both Figs. 4 and 5 are $k_0\hat{R}_b = 0.1$, $\gamma_b = 2$, $\alpha_{0\ell} = 3.83$ $(\ell = 1)$, $\hat{V}_{\perp b}/c = 0.1$, $V_b/c = 0.866$, $\omega_{pb}/ck_0 = 0.25$, and $\delta B/B_0 = 1/3$. In Fig. 4, we have chosen the parameter $(\delta B/B_0)(\omega_{cb}/ck_0) = \alpha_{1,1} = 1.841$, which maximizes the growth rate for $n = 1$. On the other hand, in Fig. 5 we have chosen $(\delta B/B_0)(\omega_{cb}/ck_0) = \alpha_{3,1} = 4.201$, which maximizes the growth rate for $n = 3$. For example, comparing Figs. 4(a) and 5(a), we note that there is a considerable upshift in maximum growth from normalized wavenumber $k/k_0 = 31.5$ in Fig. 4(a) $(n = 1)$ to $k/k_0 = 97.3$ in Fig. 5(a) $(n = 3)$, as the parameter $(\delta B/B_0)(\omega_{cb}/ck_0)$ is increased from 1.841 to 4.201. Figures 4 and 5 also illustrate the strong dependence of growth rate on finite radial geometry. In particular, the plots

in Figs. 4(a) and 5(a) are presented for the case where the conducting wall is relatively close to the electron beam ($\hat{R}_b/R_c = 0.25$, $g_1 = 3.792 \times 10^{-2}$, and $g_2 = 1.314 \times 10^{-2}$), whereas the plots in Figs. 4(b) and 5(b) correspond to the case where the conducting wall is much further removed from the electron beam ($\hat{R}_b/R_c = 0.1$, $g_1 = 1.105 \times 10^{-3}$, and $g_2 = 3.704 \times 10^{-4}$). As $\hat{R}_b/R_c$ is decreased, we note that there is both an upshift in the value of k/k_0 corresponding to maximum growth as well as a significant reduction in growth rate. [Compare Figs. 4(a) and 4(b) or Figs. 5(a) and 5(b).] It is clear from the analytic results in Secs. IV.A and IV.B and the numerical results in Figs. 4 and 5, that there is a strong influence of radial geometry on the growth properties of the longitudinal wiggler free electron laser. Indeed, as expected from Figs. 2 and Eqs. (60) and (61), the closer the conducting wall (R_c) is positioned to the beam radius ($\hat{R}_b$), the larger the instability growth rate becomes. Of course, this is associated with the fact that g_2 increases as $\hat{R}_b/R_c$ is increased [Fig. 2 and Eq. (54)]. Another striking feature of Figs. 4 and 5 is that the instability is relatively broadband. Even though $(\delta B/B_0)(\omega_{cb}/ck_0)$ is chosen to maximize $Im\omega$ for a particular value of n, adjacent harmonics still have relatively strong growth. (See also the discussion at the end of Sec. IV.B).

Cyclotron Maser Instability: In the limiting case where $\delta B = 0$ and the applied magnetic field is given by the uniform value $B_0\hat{e}_z$, only the $n = 0$ term survives in Eq. (60) with $J_0^2(0) = 1$. The resulting dispersion relation applies to the cyclotron maser instability for the choice of solid electron beam equilibrium distribution in Eqs. (6) and (16). The dispersion relation (60) has been solved numerically for the growth rate $Im\omega$ assuming $\delta B = 0$. Typical results are summarized in Fig. 6, where the normalized growth rate $Im\omega/\omega_{cb}$ is plotted versus $k\hat{R}_b$ for the choice of parameters

$\gamma_b = 2$, $\alpha_{0\ell} = 3.83$ ($\ell = 1$), $\hat{V}_{\perp b}/c = 0.1$, $V_b/c = 0.866$ and $\omega_{pb}/\omega_{cb} = 2.29 \times 10^{-2}$. To illustrate the influence of finite radial geometry, we have chosen $\hat{R}_b/R_c = 0.25$ in Fig. 6(a) (corresponding to $g_1 = 3.792 \times 10^{-2}$ and $g_2 = 1.314 \times 10^{-2}$) and $\hat{R}_b/R_c = 0.1$ in Fig. 6(b) (corresponding to $g_1 = 1.105 \times 10^{-3}$ and $g_2 = 3.704 \times 10^{-4}$). As for the case of the longitudinal wiggler free electron laser ($\delta B \neq 0$), it is clear from Fig. 6 that the relative positioning of the beam radius ($\hat{R}_b$) and the conducting wall radius (R_c) also has a large influence on the strength of the cyclotron maser instability. Indeed, the growth rate increases as $\hat{R}_b/R_c$ is increased. [Compare Figs. 6(a) and 6(b).] As in Figs. 4 and 5, there is a concommitant upshift in k/k_0 corresponding to maximum growth as $\hat{R}_b/R_c$ is decreased.

V. CONCLUSIONS

In this paper, we have investigated the influence of finite radial geometry on the longitudinal wiggler free electron laser instability.[1] The analysis is carried out for a thin, tenuous electron beam propagating down the axis of a multiple-mirror (undulator) magnetic field (Sec. III). It is assumed that $k_0^2\hat{R}_b^2 \ll 1$ and that the amplifying radiation field has TE-mode polarization with perturbed field components ($\delta\hat{E}_\theta$, $\delta\hat{B}_r$, $\delta\hat{B}_z$). A very important feature of the linear stability analysis (Secs. III and IV) is that the positioning of the beam radius relative to the conducting wall radius (as measured by $\hat{R}_b/R_c$, say) can have a large influence on the growth rate and detailed stability properties for perturbations about the choice of equilibrium distribution $f_b^0(\underset{\sim}{x},\underset{\sim}{p})$ in Eq. (16).

Several points are noteworthy from the stability analysis in Sec. IV. First, for a given harmonic number n, the characteristic maximum growth rate [Eq. (68)] is largest whenever the argument of J_n corresponds to the first zero of $J_n'(x) = 0$, i.e., when $(\omega_{cb}/k_0V_b)(\delta B/B_0) = \alpha_{n,1}$, where $\alpha_{n,1}$ is the first zero of $J_n'(x) = 0$. Second, the growth rate scales as $(\hat{V}_{\perp b}/c)^{2/3}\hat{n}_b^{1/3}$, which can lead to substantial gain for the longitidunal wiggler free electron laser. Third, there is a strong dependence of stability properties on the positioning of the beam radius ($\hat{R}_b$) relative to the conducting wall radius (R_c). In particular, the growth rate Imω increases as $\hat{R}_b/R_c$ is increased, and the detailed dependence of Imω on $\hat{R}_b/R_c$ was examined numerically in Sec. IV. Another important feature of the results is that the instability is inherently broadband in the sense that many harmonics are unstable, even when $(\omega_{cb}/k_0V_b)(\delta B/B_0)$ is chosen to maximize emission for a particular value of n.

Finally, also in Sec. IV, we investigated stability properties in the limiting case where $\delta B = 0$. This corresponds the cyclotron maser instability for perturbations about the solid electron beam equilibrium $f_b^0(\underset{\sim}{x},\underset{\sim}{p})$ specified by Eq. (16). The numerical results for $\delta B = 0$ also exhibited a strong dependence on radial geometry $(\hat{R}_b/R_c)$.

ACKNOWLEDGMENTS

This research was supported by the Office of Naval Research.

REFERENCES

1. R.C. Davidson and W.A. McMullin, Phys. Fluids 26, 840 (1983).
2. R.C. Davidson and W.A. McMullin, Phys. Rev. A26, 1997 (1982).
3. W.A. McMullin and G. Bekefi, Phys. Rev. A25, 1826 (1982).
4. W.A. McMullin and G. Bekefi, Appl. Phys. Lett. 39, 845 (1981).
5. H.S. Uhm and R.C. Davidson, Phys. Fluids 24, 1541 (1981).
6. V.P. Sukhatme and P.A. Wolff, J. Appl. Phys. 44, 2331 (1973).
7. W.B. Colson, Phys. Lett. 59A, 187 (1976).
8. T. Kwan, J.M. Dawson, and A.T. Lin, Phys. Fluids 20, 581 (1977).
9. N.M. Kroll and W.A. McMullin, Phys. Rev. A17, 300 (1978).
10. T. Kwan and J.M. Dawson, Phys. Fluids 22, 1089 (1979).
11. I.B. Bernstein and J.L. Hirshfield, Physica (Utrecht) 20A, 1661 (1979).
12. P. Sprangle and R.A. Smith, Phys. Rev. A21, 293 (1980).
13. R.C. Davidson and H.S. Uhm, Phys. Fluids, 23, 2076 (1980).
14. W.B. Colson, IEEE J. Quant. Electron. QE17, 1417 (1981).
15. G.L. Johnston and R.C. Davidson, J. Appl. Phys. 55, 1285 (1984).
16. H.S. Uhm and R.C. Davidson, Phys. Fluids 24, 2348 (1981).
17. H.S. Uhm and R.C. Davidson, Phys. Fluids 26, 288 (1983).
18. R.C. Davidson, W.A. McMullin and K. Tsang, Phys. Fluids 27, 233 (1983).
19. F.A. Hopf, P. Maystre, M.O. Scully, and W.H. Louisell, Phys. Rev. Lett. 37, 1342 (1976).
20. W.H. Louisell, J.F. Lam, D.A. Copeland, and W.B. Colson, Phys. Rev. A19, 288 (1979).
21. P. Sprangle, C.M. Tand, and W.M. Manheimer, Phys. Rev. A21, 302 (1980).
22. N.M. Kroll, P.L. Morton, and M.N. Rosenbluth, IEEE J. Quantum Electron. QE17, 1436 (1981).
23. T. Tagushi, K. Mima, and T. Mochizuki, Phys. Rev. Lett. 46, 824 (1981).
24. N.S. Ginzburg and M.A. Shapiro, Opt. Comm. 40, 215 (1982).

25. R.C. Davidson and W.A. McMullin, Phys. Rev. A26, 410 (1982).

26. B. Lane and R.C. Davidson, Phys. Rev. A27, 2008 (1983).

27. L.R. Elias, W.M. Fairbank, J.M.J. Madey, H.A. Schwettman, and T.I. Smith, Phys. Rev. Lett. 36, 717 (1976).

28. D.A.G. Deacon, L.R. Elias, J.M.J. Madey, G.J. Ramian, H.A. Schwettman, and T.I. Smith, Phys. Rev. Lett. 38, 892 (1977).

29. D.B. McDermott, T.C. Marshall, S.P. Schlesinger, R.K. Parker, and V.L. Granatstein, Phys. Rev. Lett. 41, 1368 (1978).

30. A.N. Didenko, A.R. Borisov, G.R. Fomenko, A.V. Kosevnikov, G.V. Melnikov, Yu G. Stein, and A.G. Zerlitsin, IEEE Trans. Nucl. Sci. 28, 3169 (1981).

31. S. Benson, D.A.G. Deacon, J.N. Eckstein, J.M.J. Madey, K. Robinson, T.I. Smith, and R. Taber, Phys. Rev. Lett. 48, 235 (1982).

32. R.K. Parker, R.H. Jackson, S.H. Gold, H.P. Freund, V.L. Granatstein, P.C. Efthimion, M. Herndon, and A.K. Kinkead, Phys. Rev. Lett. 48, 238 (1982).

33. A. Grossman, T.C. Marshall, IEEE J. Quant. Electron. QE19, 334 (1983).

34. G. Bekefi, R.E. Shefer and W.W. Destler, Appl. Phys. Lett. 44, 280 (1983).

35. J. Fajans, G. Bekefi, Y.Z. Yin, and B. Lax, "Spectral Measurements from a Tunable, Raman, Free Electron Maser," MIT Plasma Fusion Center Report #JA-84-4 (1984).

36. R.C. Davidson, G.L. Johnston and W.A. McMullin, Phys. Rev. A29, in press (1984).

37. H.S. Uhm, R.C. Davidson, and K.R. Chu, Phys. Fluids 21, 1866 (1978).

38. H.S. Uhm, R.C. Davidson, and K.R. Chu, Phys. Fluids 21, 1877 (1978).

39. H.S. Uhm and R.C. Davidson, J. Appl. Phys. 50, 696 (1979).

FIGURE CAPTIONS

Fig. 1 Longitudinal wiggler free electron laser configuration and coordinate system.

Fig. 2 Plot of geometric factors (a) g_1 [Eq. (53)] and (b) g_2 [Eq. (54)] versus $\hat{R}_b/R_c$ for several values of ℓ.

Fig. 3 Plot of ω/ck_0 versus k/k_0 obtained from Eq. (62) for $\gamma_b = 2$, $V_b/c = 0.866$, $\alpha_{0\ell} = 3.83$, $\omega_{cb}/ck_0 = 4.78$ and $k_0R_c = 0.4$. The upshifted interception points $(\hat{\omega}_n, \hat{k}_n)$ correspond to Eqs. (63) and (64), where $k_{\perp\ell} = \alpha_{0\ell}/R_c$.

Fig. 4 Plot of normalized growth rate $Im\omega/ck_0$ versus k/k_0 obtained numerically from Eq. (60) for $k_0\hat{R}_b = 0.1$, $\gamma_b = 2$, $\hat{V}_{\perp b}/c = 0.1$, $V_b/c = 0.866$, $\alpha_{0\ell} = 3.83$ $(\ell = 1)$, $\omega_{pb}/ck_0 = 0.25$, $\delta B/B_0 = 1/3$, and $(\delta B/B_0)(\omega_{cb}/k_0V_b) = 1.841$ for (a) $k_0R_c = 0.4$, $\hat{R}_b/R_c = 0.25$, $g_1 = 3.792 \times 10^{-2}$ and $g_2 = 1.314 \times 10^{-2}$, and for (b) $k_0R_c = 1.0$, $\hat{R}_b/R_c = 0.1$, $g_1 = 1.105 \times 10^{-3}$ and $g_2 = 3.704 \times 10^{-4}$.

Fig. 5 Plot of normalized growth rate $Im\omega/ck_0$ versus k/k_0 obtained numerically from Eq. (60) for $k_0\hat{R}_b = 0.1$, $\gamma_b = 2$, $\hat{V}_{\perp b}/c = 0.1$, $V_b/c = 0.866$, $\alpha_{0\ell} = 3.83$ $(\ell = 1)$, $\omega_{pb}/ck_0 = 0.25$, $\delta B/B_0 = 1/3$, and $(\delta B/B_0)(\omega_{cb}/ck_0) = 4.201$ for (a) $k_0R_c = 0.4$, $\hat{R}_b/R_c = 0.25$, $g_1 = 3.792 \times 10^{-2}$ and $g_2 = 1.314 \times 10^{-2}$, and for (b) $k_0R_c = 1.0$, $\hat{R}_b/R_c = 0.1$, $g_1 = 1.105 \times 10^{-3}$ and $g_2 = 3.704 \times 10^{-4}$.

Fig. 6 Plot of normalized cyclotron maser growth rate $\mathrm{Im}\omega/\omega_{cb}$ versus $k\hat{R}_b$ obtained numerically from Eq. (60) for $\delta B = 0$, $\gamma_b = 2$, $V_{\perp b}/c = 0.1$, $V_b/c = 0.866$, $\alpha_{0\ell} = 3.83$ ($\ell = 1$), and $\omega_{pb}/\omega_{cb} = 2.29 \times 10^{-2}$ for (a) $\hat{R}_b/R_c = 0.25$, $g_1 = 3.792 \times 10^{-2}$ and $g_2 = 1.314 \times 10^{-2}$, and for (b) $\hat{R}_b/R_c = 0.1$, $g_1 = 1.105 \times 10^{-3}$ and $g_2 = 3.704 \times 10^{-4}$.

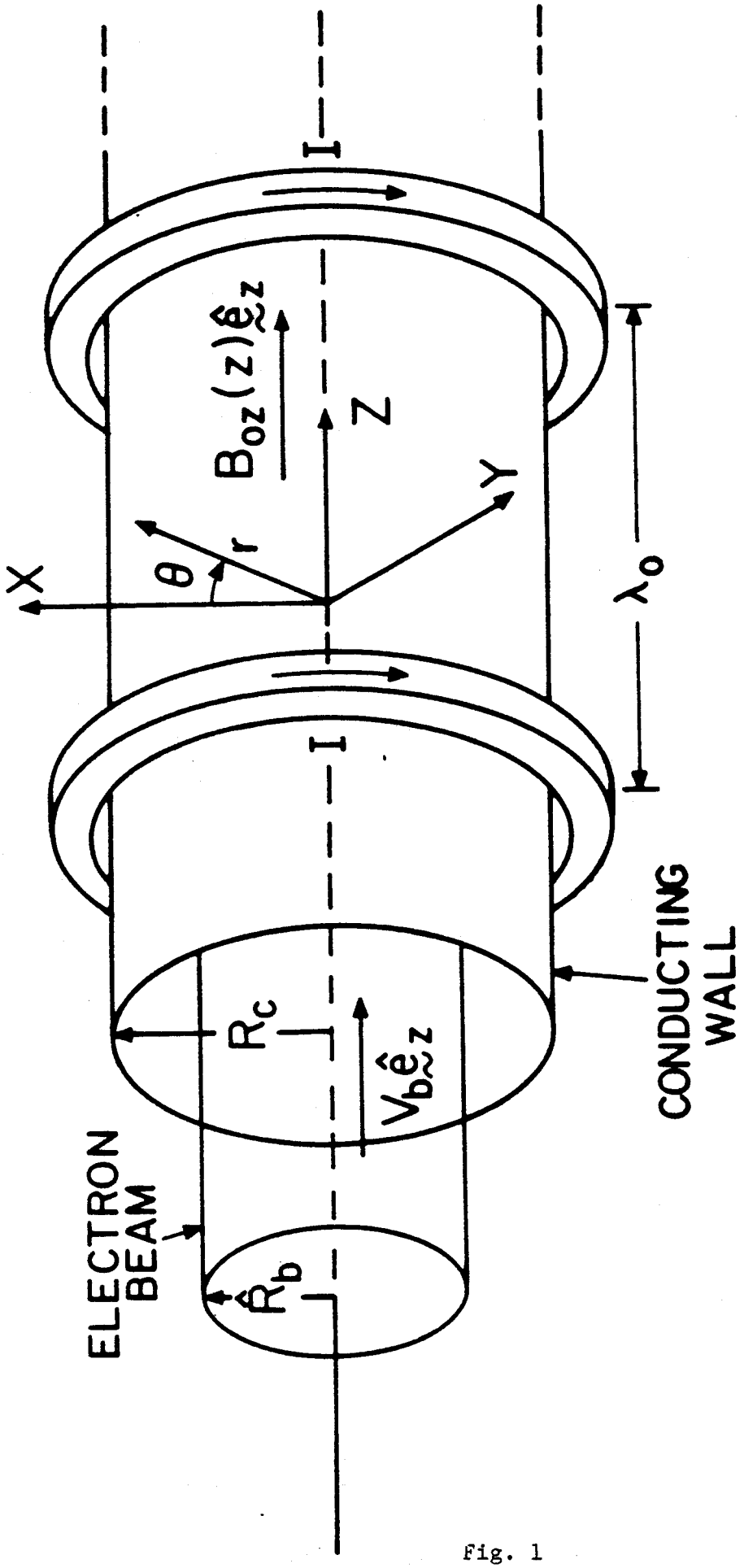
I
$B_{oz}(z)\hat{e}_z$
Z
Y
X
θ
r
λ_o
I
CONDUCTING WALL
R_c
$V_b\hat{e}_z$
ELECTRON BEAM
R_b

Fig. 1

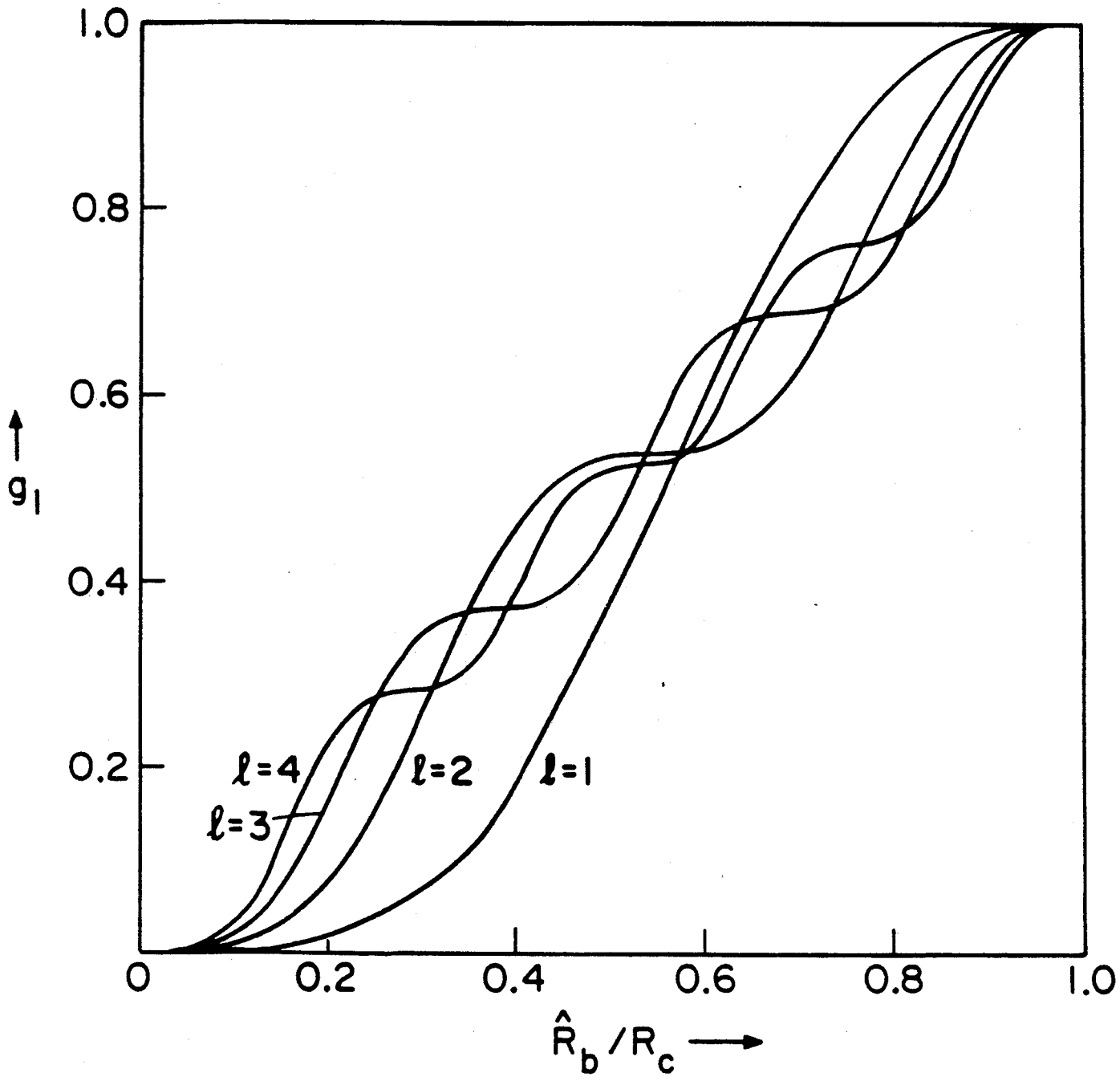

Fig. 2(a)

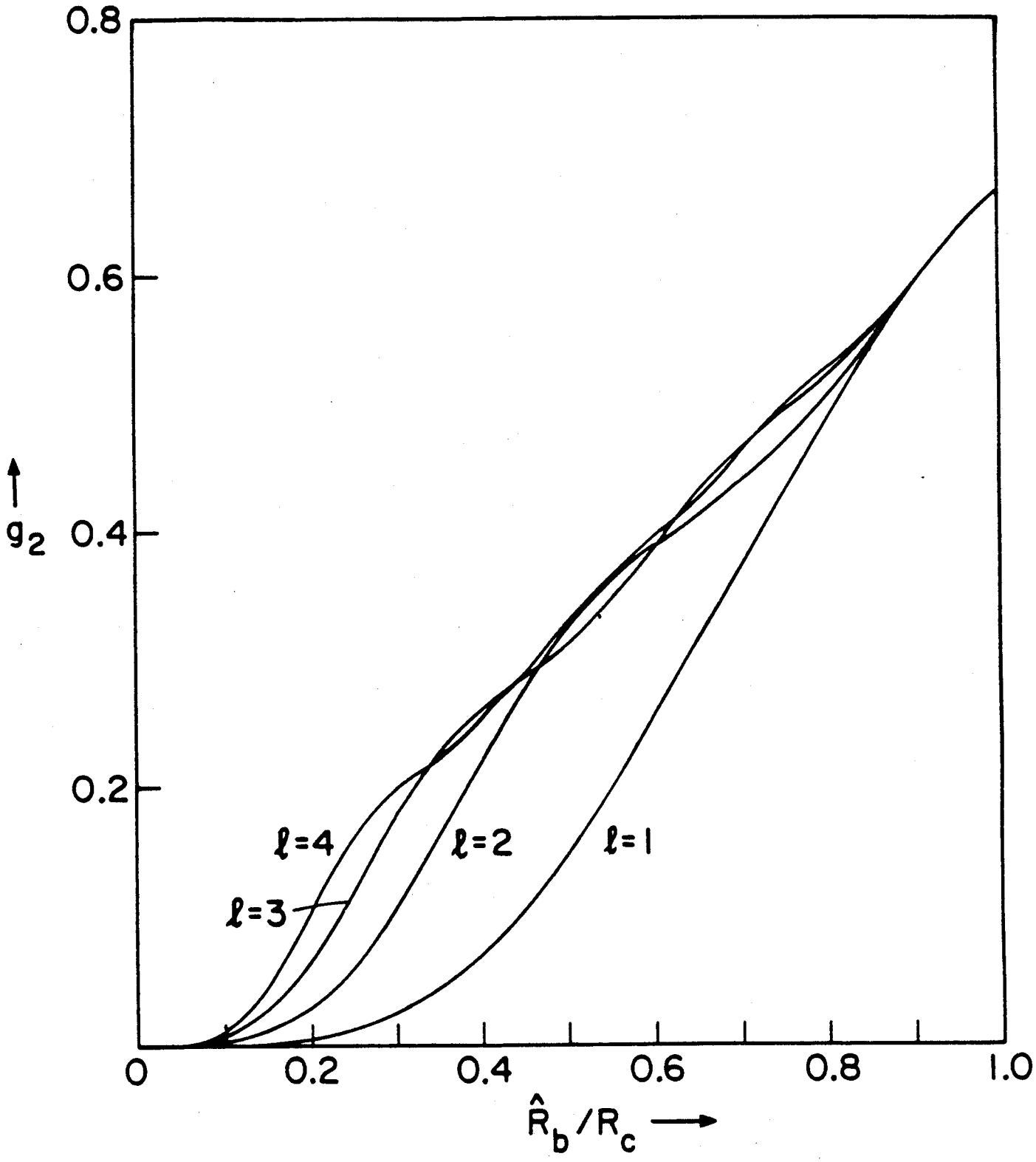

Fig. 2(b)

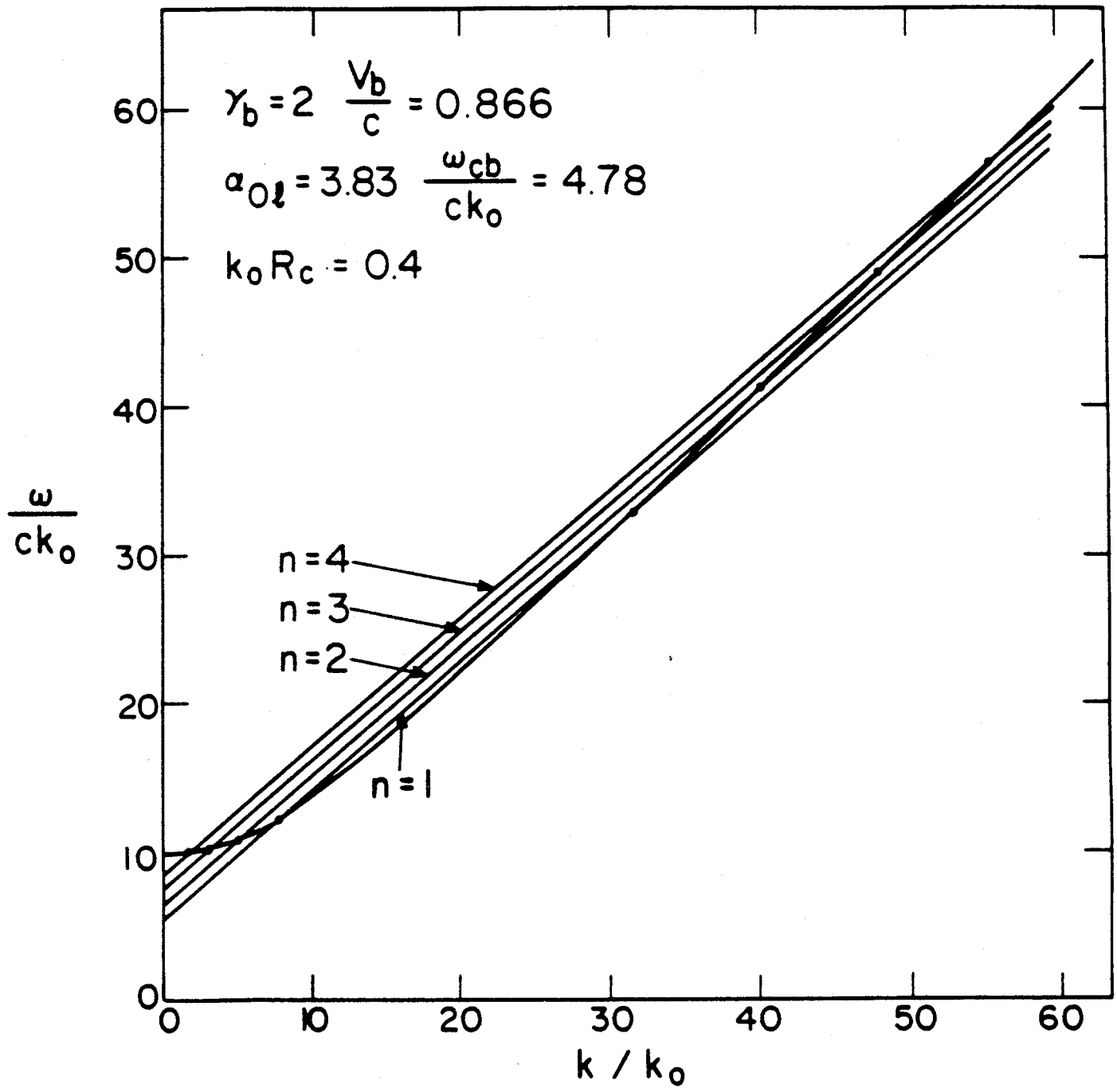
$\gamma_b = 2$ $\frac{V_b}{c} = 0.866$
$\alpha_{0\ell} = 3.83$ $\frac{\omega_{cb}}{ck_0} = 4.78$
$k_0 R_c = 0.4$
n = 4
n = 3
n = 2
n = 1
$\frac{\omega}{ck_0}$
k / k_0
0
10
20
30
40
50
60

Fig. 3

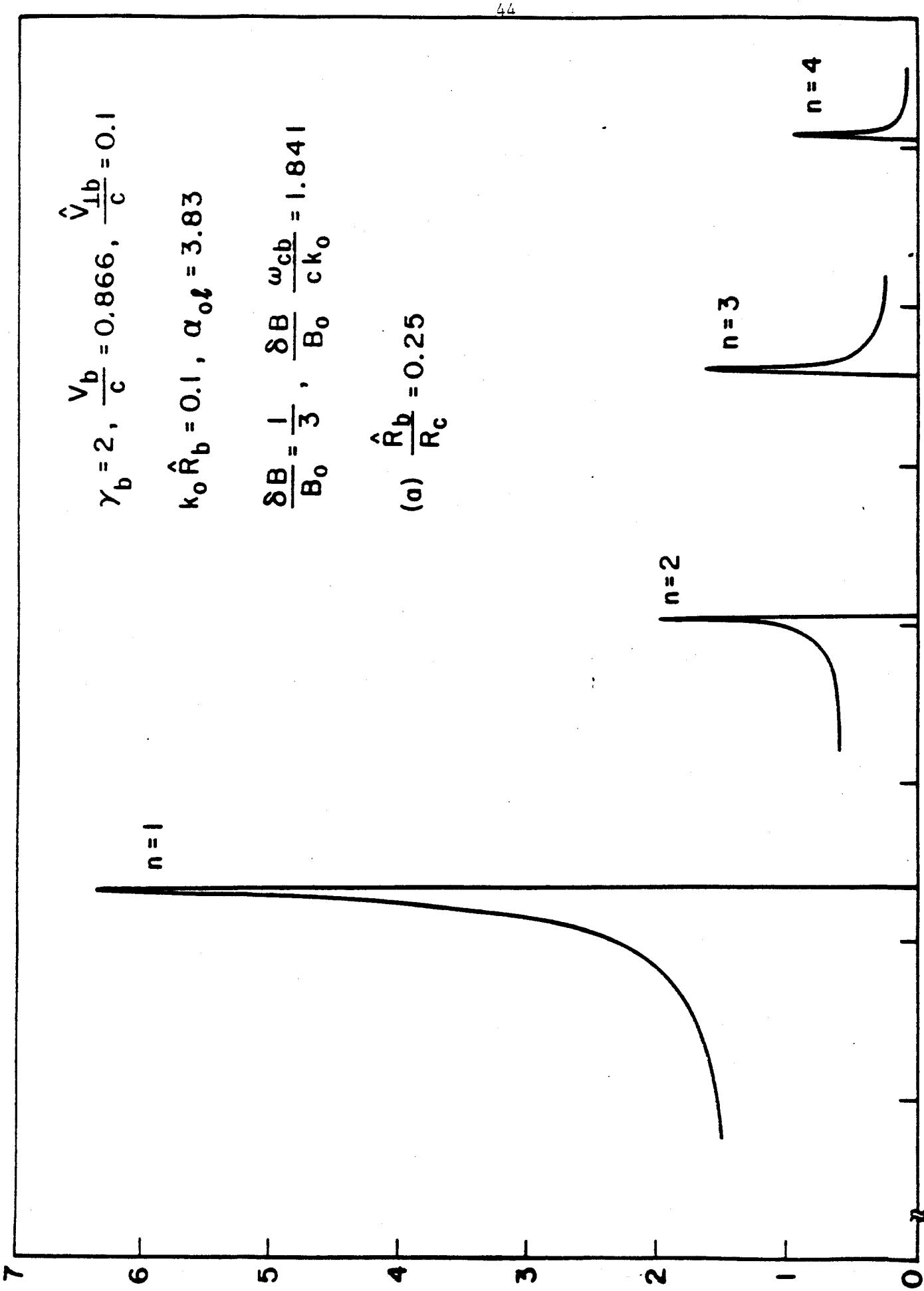
$\gamma_b = 2$, $\frac{V_b}{c} = 0.866$, $\frac{\hat{V}_{\perp b}}{c} = 0.1$
$k_o \hat{R}_b = 0.1$, $\alpha_{o\ell} = 3.83$
$\frac{\delta B}{B_o} = \frac{1}{3}$, $\frac{\delta B}{B_o} \frac{\omega_{cb}}{c k_o} = 1.841$
(a) $\frac{\hat{R}_b}{R_c} = 0.25$
n=1
n=2
n=3
n=4
10^3 Im ω/ck_o
k/k_o
0
1
2
3
4
5
6
7
25
30
35
40
45
50
55

Fig. 4(a)

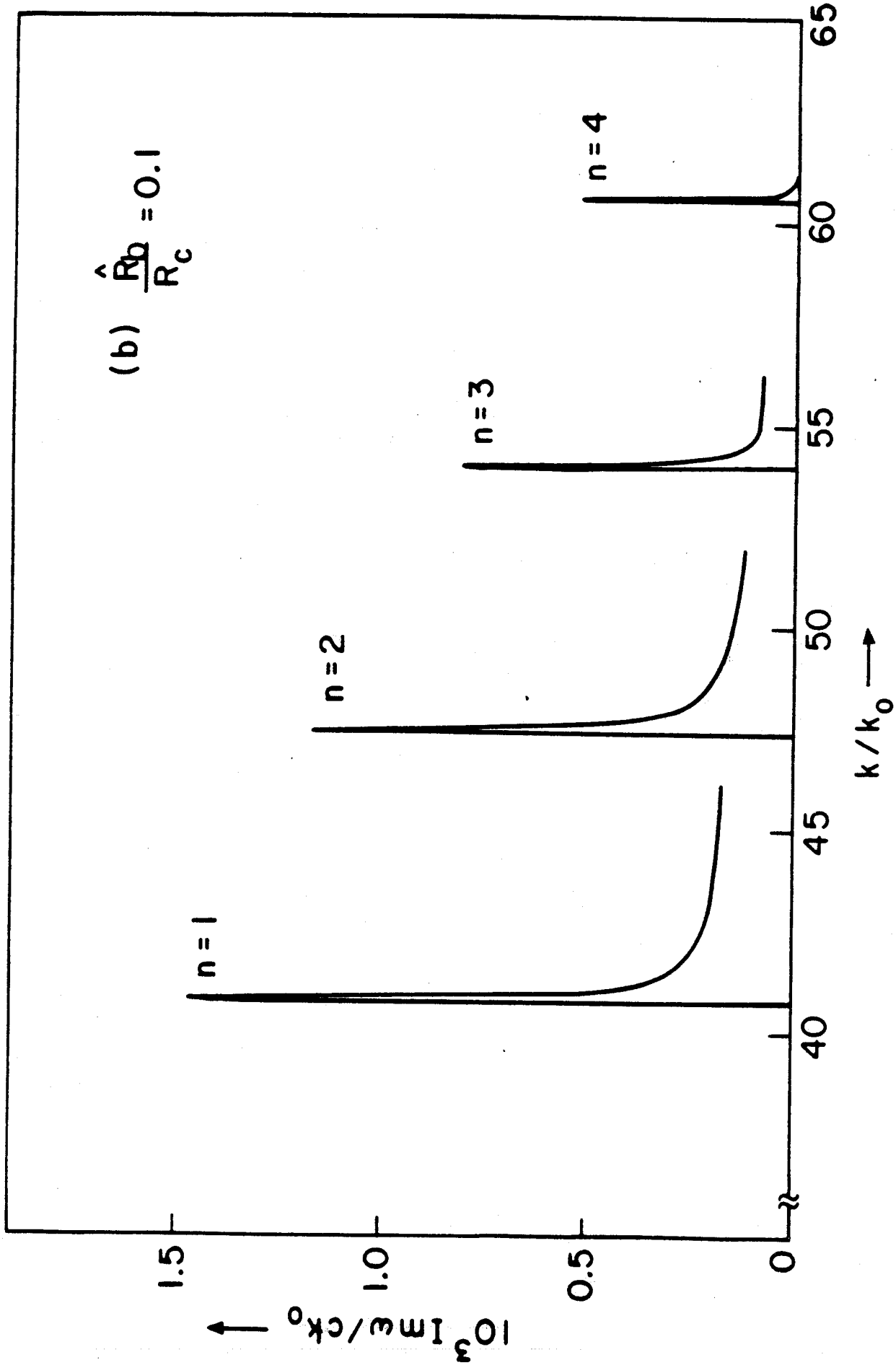
(b) $\frac{\hat{R}_b}{R_c} = 0.1$
n=1
n=2
n=3
n=4
$10^3 \mathrm{Im}\omega/ck_o$
k/k_o
0
0.5
1.0
1.5
40
45
50
55
60
65

Fig. 4(b)

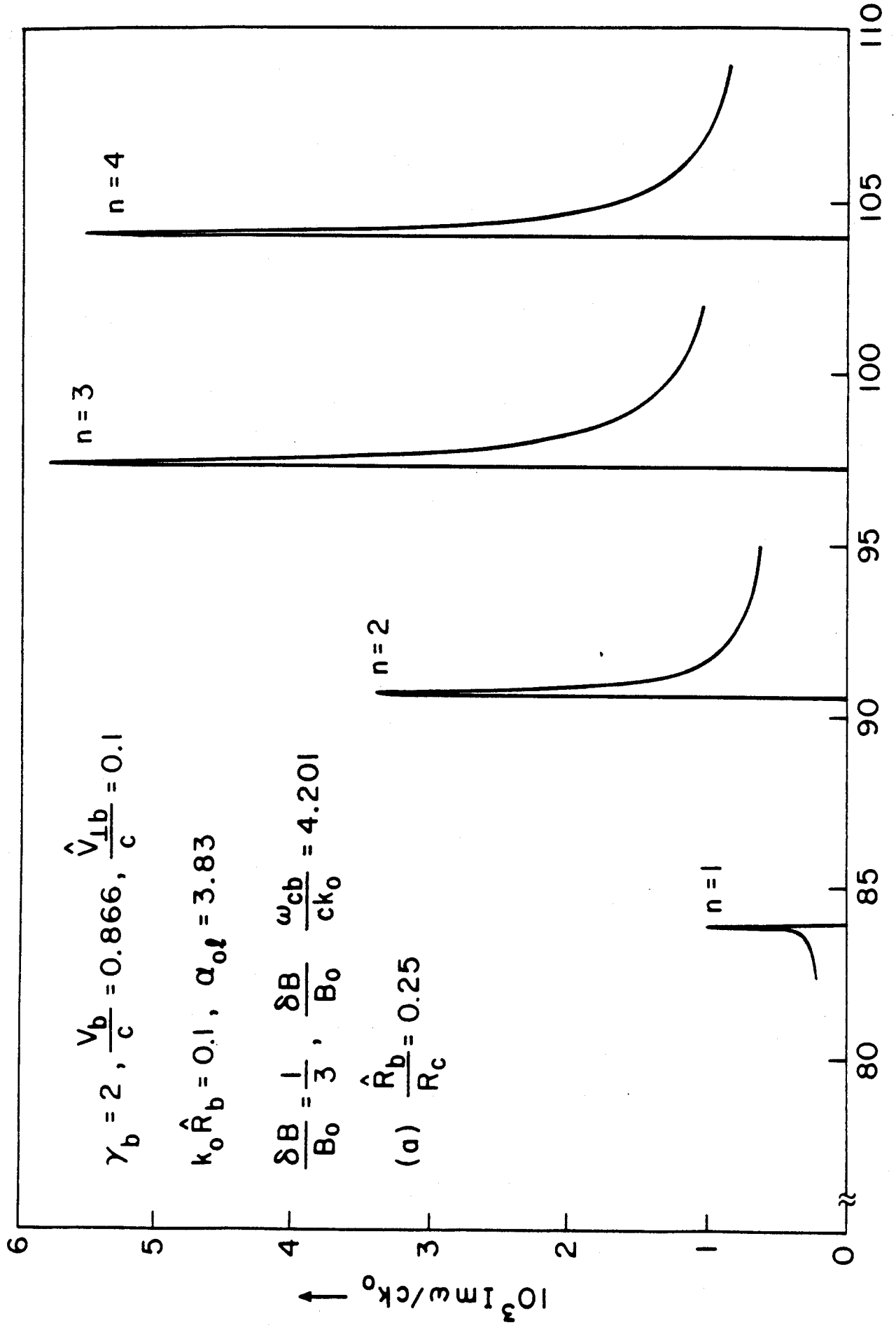
$\gamma_b = 2$, $\frac{V_b}{c} = 0.866$, $\frac{\hat{V}_{\perp b}}{c} = 0.1$
$k_o \hat{R}_b = 0.1$, $\alpha_{o\ell} = 3.83$
$\frac{\delta B}{B_o} = \frac{1}{3}$, $\frac{\delta B}{B_o}$ $\frac{\omega_{cb}}{ck_o} = 4.201$
(a) $\frac{\hat{R}_b}{R_c} = 0.25$
n = 1
n = 2
n = 3
n = 4
$10^3 \, Im\omega/ck_o$ ⟶
k/k_o ⟶
0
1
2
3
4
5
6
80
85
90
95
100
105
110

Fig. 5(a)

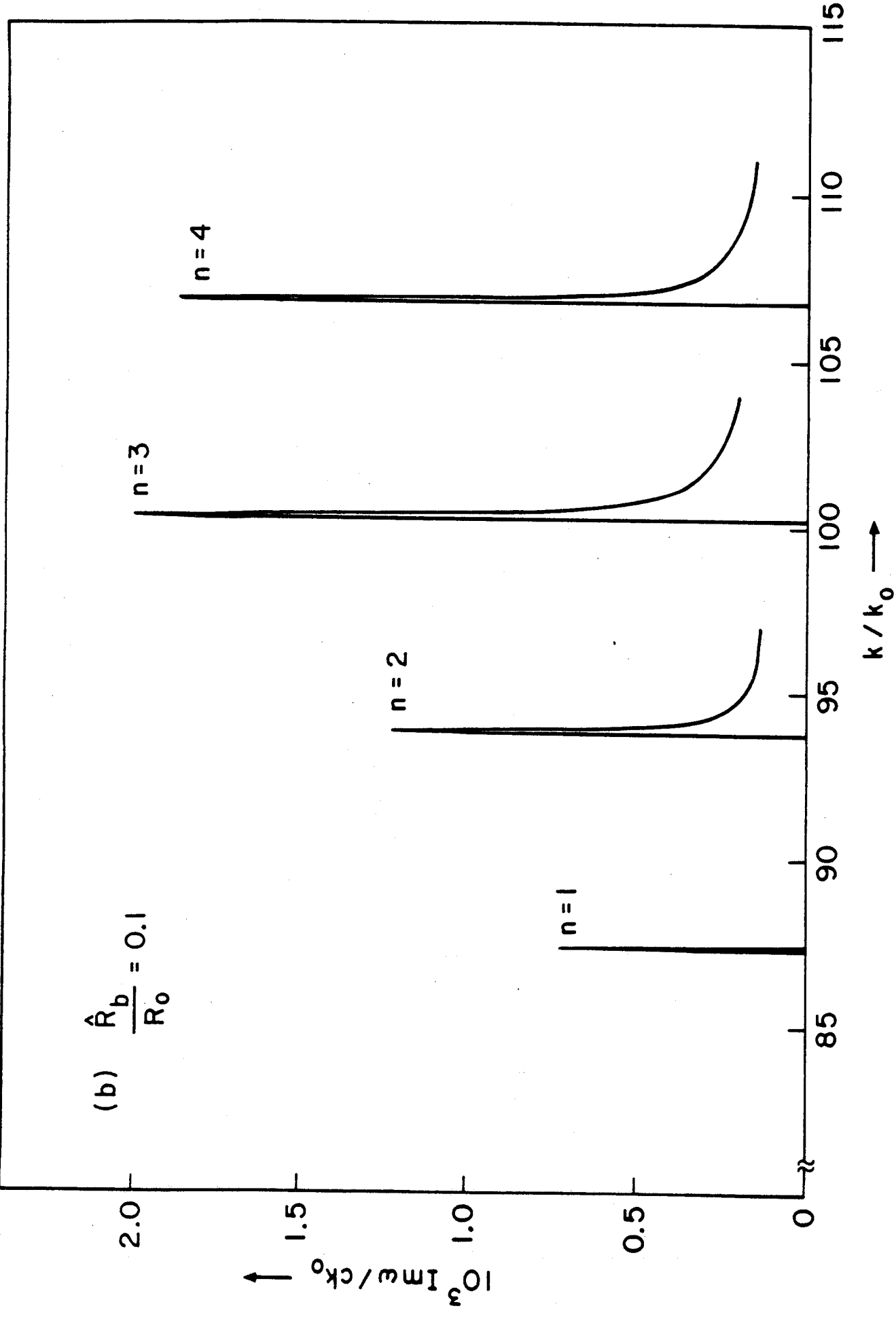
(b) $\frac{\hat{R}_b}{R_o} = 0.1$
n = 1
n = 2
n = 3
n = 4
$10^3\ \mathrm{Im}\omega/ck_o$ ⟵
k/k_o ⟶
0
0.5
1.0
1.5
2.0
85
90
95
100
105
110
115

Fig. 5(b)

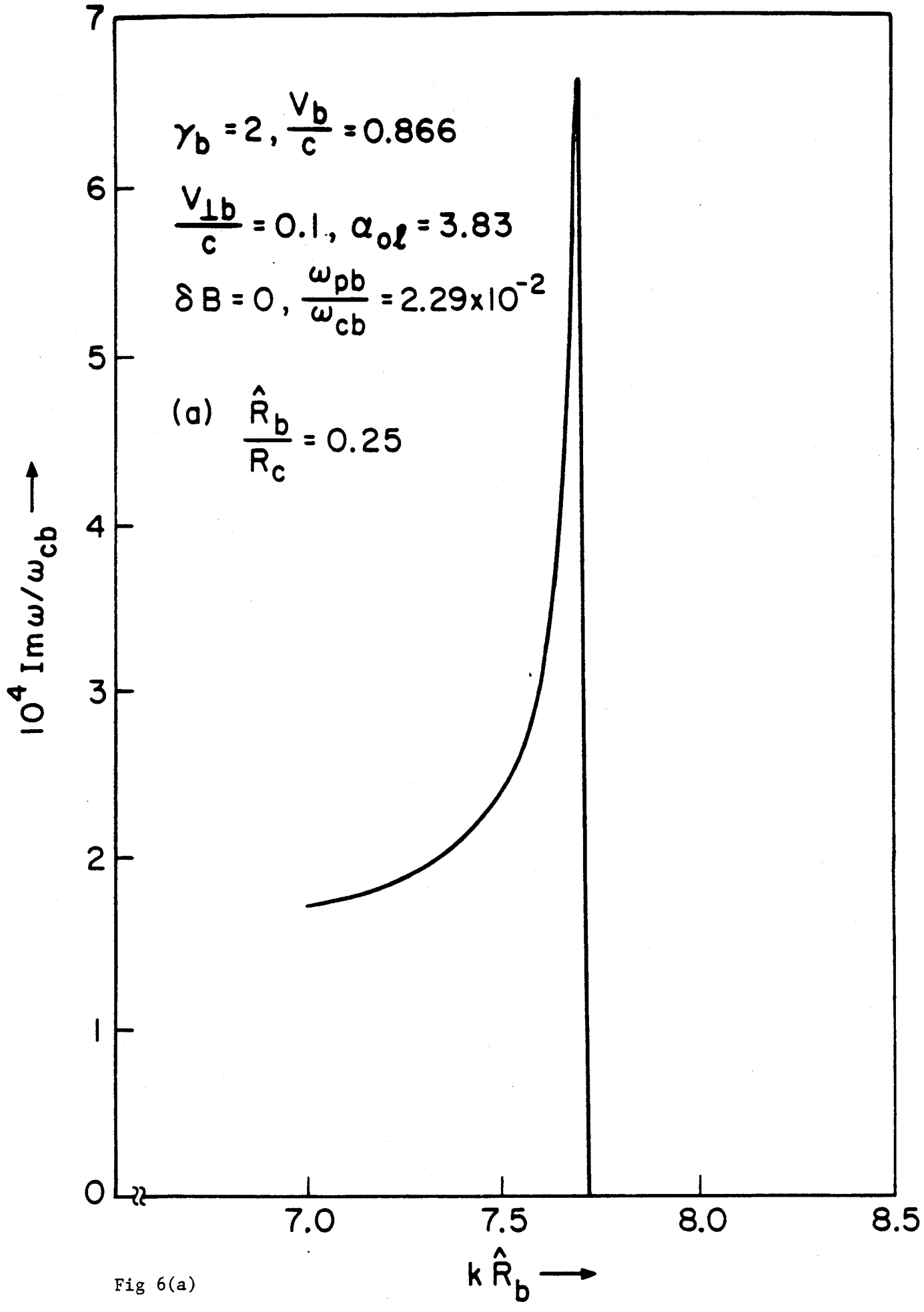
$\gamma_b = 2, \frac{V_b}{c} = 0.866$
$\frac{V_{\perp b}}{c} = 0.1, \alpha_{o\ell} = 3.83$
$\delta B = 0, \frac{\omega_{pb}}{\omega_{cb}} = 2.29 \times 10^{-2}$
(a) $\frac{\hat{R}_b}{R_c} = 0.25$
$10^4\, Im\,\omega/\omega_{cb}$
$k\hat{R}_b$
0
1
2
3
4
5
6
7
7.0
7.5
8.0
8.5

Fig 6(a)

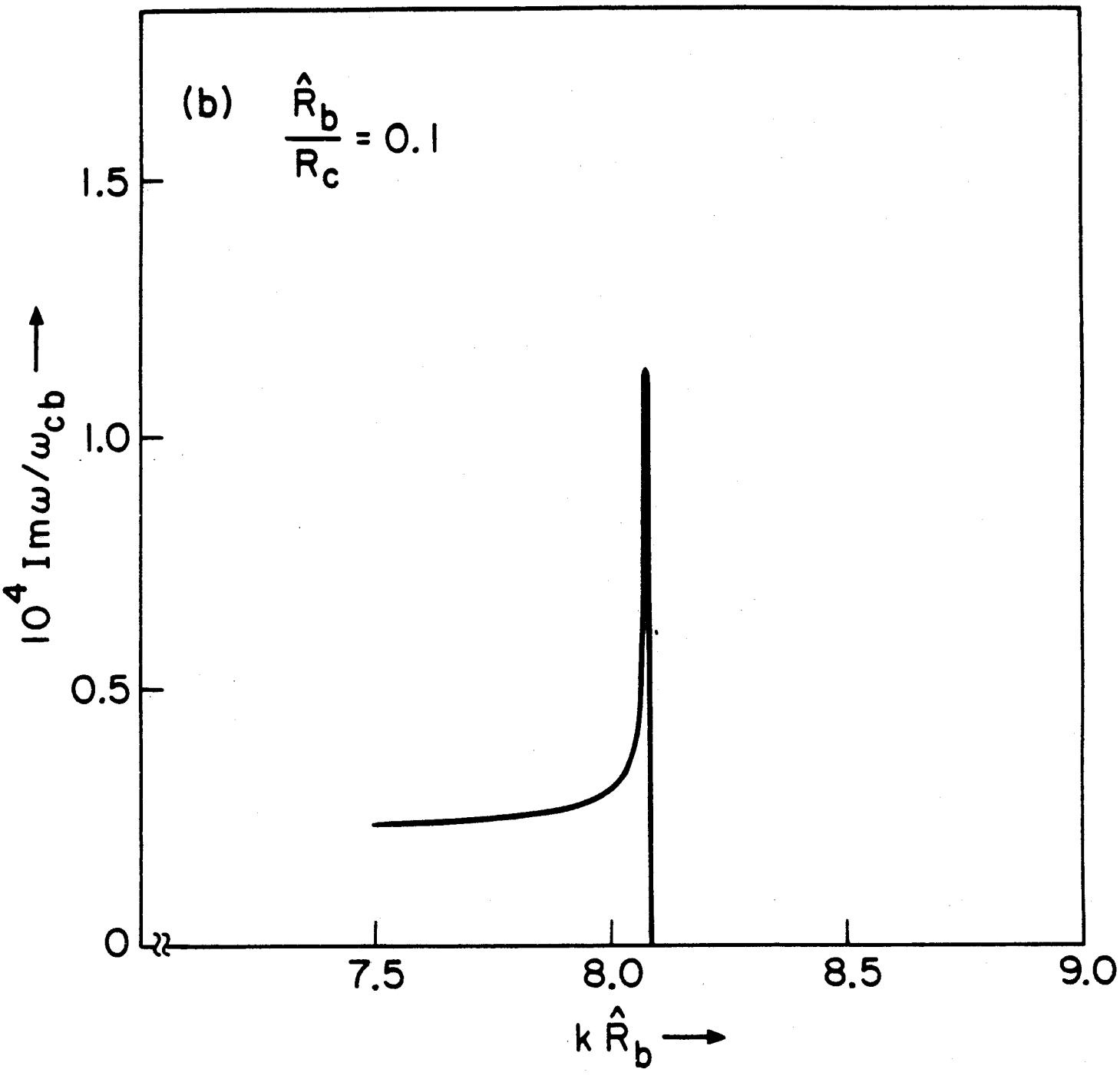
(b) $\frac{\hat{R}_b}{R_c} = 0.1$
1.5
1.0
0.5
0
$10^4 \, Im\omega/\omega_{cb}$
7.5
8.0
8.5
9.0
$k\hat{R}_b$

Fig. 6(b)